La Palma landslide tsunami: computation of the tsunami source with a calibrated multi-fluid Navier-Stokes model and wave impact assessment with propagation models of different types

Stéphane Abadie[1], Alexandre Paris[1,2,3], Riadh Ata[4], Sylvestre Le Roy[5], Gael Arnaud[6], Adrien Poupardin[2,3], Lucie Clous[1], Philippe Heinrich[3], Jeffrey Harris[4], Rodrigo Pedreros[5], and Yann Krien[6]

[1]UNIV PAU & PAYS ADOUR/ E2S UPPA, Laboratoire des Sciences de l'Ingénieur Appliquées à la Mécanique et au Génie Electrique, Fédération IPRA, EA4581, 64600, ANGLET, France
[2]Laboratoire de Géologie, Ecole normale supérieure/CNRS UMR8538, PSL Research University, Paris, France
[3]CEA, DAM, DIF, Arpajon 91297, France
[4]LHSV, Ecole des Ponts, CEREMA, EDF R et D, Chatou, France
[5]BRGM, Orléans, France
[6]Université des Antilles, Laboratoire LARGE, Campus de Fouillole, 97157 Pointe-a-Pitre, Guadeloupe

Correspondence: Stephane Abadie (stephane.abadie@univ-pau.fr)

Abstract. In this paper, we present a new source assessment of the La Palma collapse scenario previously described and studied in Abadie et al. (2012). Three scenarios (*i.e.*, slide volumes of 20, 40 and 80 km^3) are considered, from the initiation of the slide to the water waves generation, using THETIS, a 3D Navier-Stokes model. The slide is considered as a Newtonian fluid whose viscosity is adjusted to approximate a granular behavior. After 5 minutes of propagation with THETIS, the generated water wave is transferred into FUNWAVE-TVD for 15 minutes of Boussinesq model simulation. Then, four different depth-averaged codes are used to propagate the wave to the Guadeloupe area, Europe and French coasts. Finally, the wave impact in terms of run-up is evaluated through direct computations in specific areas or using theoretical formulas. Although the wave source appears reduced due to the rheology used compared to former works, the wave impact is still significant for the maximum slide volume considered on surrounding islands and coasts, as well as on remote most exposed coasts such as Guadeloupe. In Europe and in France, the wave impact is moderate (for specific areas in Spain and Portugal) to weak (Atlantic French coast). The comparison between the different wave models in overlapping computational regions shows an overall agreement in terms of first wave amplitude and time of arrival, but differences appear in the trailing waves.

Keywords: Tsunamis, Atlantic Ocean, numerical modelling, Volcanic hazards and risks

1 Introduction

Recent catastrophes due to exceptionally strong tsunamis (Athukorala and Resosudarmo, 2005; Mikami et al., 2012) have called the need for extensive tsunami risk assessment or reassessment in several countries (*e.g.*, National Tsunami Hazard Mitigation Program (NTHMP) in the USA (Tehranirad et al., 2015), or the Tsunamis in the Atlantic and the English ChaNnel Definition of the Effects through numerical Modeling (TANDEM) project for France (Hebert, 2014). In this context, the risk

associated to various potentially tsunamigenic sources has to be evaluated. This work usually covers the most frequent sources, namely co-seismic displacements and submarine landslides, but less probable sources, like volcano tsunami sources, must also be investigated. Volcanic islands may indeed have the potential to generate tsunamis, even mega-tsunamis, through a flank collapse process (Tappin et al., 2019), known to occur relatively regularly (Elsworth and Day, 1999). Footprints of such

5   gigantic past events are large underwater landslide debris surrounding specific oceanic islands (Masson et al., 2002) and marine conglomerates at high elevation on the flanks of other ones (Paris et al., 2018). Unfortunately, the tsunami risk associated to volcanic islands is very difficult to determine, first due to the complexity of the processes involved, and second, due to the uncertainty on the associated return period. Nevertheless, although likely very rare, these events may have such dramatic consequences that they should be taken into account in extensive risk assessment studies. The present paper is an attempt,

10   in the framework of the previously cited TANDEM project, to assess the potential impact on France, some parts of Western Europe, and remote French territories (*i.e.*, the island of Guadeloupe) of a tsunami generated by an hypothetical collapse of the Cumbre Vieja volcano at La Palma Island (Canary Islands, Spain).

This volcano has drawn a strong interest among the scientific community since the first alarming work published on that case (Ward and Day, 2001). There have been several attempts to numerically simulate the waves generated by the Cumbre

15   Vieja collapse. The first work (Ward and Day, 2001) was severely criticized (Mader, 2001; Pararas-Carayannis, 2002) due to the allegedly extreme landslide volume considered and the linear wave model used. In more recent computations, Gisler et al. (2006) used a 3D compressible Navier-Stokes model to simulate the slide and the consecutive wave generated. An extrapolation of near field decay led the authors to conclude, as in Mader (2001), that wave height would not represent such a serious threat for the East coast of North America or South America. Starting from Gisler et al. (2006) near field solution, Løvholt et al.

20   (2008) simulate the transoceanic propagation of the tsunami source with a Boussinesq model, therefore including dispersive effects. The authors found smaller waves than Ward and Day (2001) but still potentially dangerous for the US coasts. Abadie et al. (2012) proposed a similar approach but based on a 3D multi-phase incompressible Navier-Stokes model to simulate the landslide and the generated wave. Because of the likelihood uncertainty, they propose four different sliding volumes, ranging from 20 to 450 km^3 obtained from a former slope stability study. The impact of these potential sources on US coasts was

25   studied in Tehranirad et al. (2015) in the framework of the NTHMP. It was shown that besides the initial directionality of the sources, coastal impact is mostly controlled by focusing/defocusing effects resulting from the shelf bathymetric features. Computations performed by Gisler et al. (2006) or Abadie et al. (2012) were both based on inviscid or quasi-inviscid slide flow.

In the present paper, the computations carried out in Abadie et al. (2012) are taken over and their accuracy improved by calibrating the slide fluid viscosity in order to better represent a granular slide (Sections 2.1 and 3.1). Then, the same filtering

30   process as in Abadie et al. (2012) is applied with the new wave sources to produce a wave signal which can be propagated by depth-averaged models (Sections 2.2 and 3.2). The three wave sources are then propagated using different models available in the TANDEM project (Section 2.3) to study the wave features close to specific areas in the Caribbean Sea (Section 3.3.2), in Western Europe and in France (Section 3.3.3). Wave run-up is then computed in these areas in Section 3.4. Finally results are interpreted and discussed in Section 4.

2 Method

2.1 Navier-Stokes simulation of wave source

The model used for wave source computations is the Navier-Stokes multi-fluid model THETIS already described in Abadie et al. (2010) and Abadie et al. (2012) in the context of waves generated by landslides. In this 3D model, water, slide and air

5 are simulated based on the incompressible Navier-Stokes equations for Newtonian fluids. The interfaces between phases are tracked using the VOF (volume-of-fluid) method. The same set-up as in Abadie et al. (2012) is used in this study, so the reader is referred to this former work to find more details on the model. The $\mu(I)$-rheology Jop et al. (2006) has also been implemented in THETIS. The latter has the form described by Lagrée et al. (2011) and implemented in Gerris, another Navier-Stokes code (Popinet, 2003).

10 As previously mentioned, the tsunami sources proposed in Abadie et al. (2012) were computed based on Navier-Stokes simulations using for the slide a Newtonian fluid of very low viscosity (quasi-inviscid). In 2D preliminary tests, the generated wave amplitudes were shown to increase gradually when lowering the slide viscosity. So the simulations performed in Abadie et al. (2012) represent the worst case possible with this model for a given slide volume. In the present paper, the aim is to propose a more realistic source prediction by calibrating the previous Navier-Stokes model with respect to recent experimental

15 measurements of waves generated by granular slides. The experimental results considered are: Viroulet et al. (2013) (see also Viroulet et al. (2014)) for subaerial slides and Grilli et al. (2017) for submarine slides.

Viroulet et al. (2013) conducted a 2D physical experiment with glass beads in order to represent an equivalent granular slide. This experiment was carried out in a flume of dimensions 2.20 m long, 0.4 m high and 0.2 m wide. The beads were placed initially above water on a 45° slope as in the Figure 2. Glass beads had a density of 2500 kg·m^{-3} and a diameter of 1.5 mm in

20 the first case, 10 mm in the second. Water depth was 14.8 cm and 15 cm for the first and second case, respectively. Four gauges monitored the surface elevation at $x_1 = 0.45$ m, $x_2 = 0.75$ m, $x_3 = 1.05$ m and $x_4 = 1.35$ m.

Numerically, the slide is modeled as a fluid with a Newtonian rheology. Simulations with a $\mu(I)$-rheology were also performed. The space and time steps are $\Delta x = 5$ mm, $\Delta y = 2$ mm and $\Delta t = 10^{-3}$ s, respectively. The flow is solved with the projection algorithm and a VOF-TVD (Total Variation Diminishing) interface tracking is performed.

25 For the first case, simulations with different values of viscosity were carried out. Figure 3 compares the height of the first wave at the four gauges. The wave simulated with the lowest viscosity (as in Abadie et al. (2012)) appears to be almost twice as high as the experimental results. This first result shows the need to consider a better calibration of the model to produce more realistic results in the La Palma case. The first wave and the wave train which follows are well reproduced for a viscosity of 10 Pa·s, even if the slide at this viscosity is shown to be slower than in the experiment. The same overall behavior is observed in

30 the second case, with glass beads diameter of 10 mm, but a higher value of viscosity has to be set in order to fit the experimental wave heights. Note that the slide motion simulated is still slower than in the experiment. This may be due to the one-fluid model formulation, which does not allow for the flow to pass through the granular medium as in reality. Energy transfers from slide to free surface, not detailed in the present study, were computed based on numerical results (Clous and Abadie, 2019) and show

that waves are generated extremely quickly in this subaerial experiment. This is certainly why the differences observed in slide velocity after some time do not induce large wave discrepancies.

The first benchmark case was also simulated with the $\mu(I)$-rheology using parameters of the literature: $\mu_s = 0.43$, $\Delta\mu = 0.39$, $I_0 = 0.27$. The results show that the wave height is quite close to the experimental results. Comparing to the computation
5   with the Newtonian fluid, during the first 0.5 s, where the waves are generated, the equivalent viscosity calculated with $\mu(I)$-rheology is quite homogeneous within the slide volume and close to the best Newtonian case. Therefore, this simulation shows that a well-calibrated Newtonian rheology can be used to model a complex granular rheology at least in this specific case for which energy transfers are very fast. This will be the approach used in the present paper.

The experiment presented in Grilli et al. (2017) was also simulated using THETIS. The experiment consisted of 2 kg of 4
10   mm glass beads released underwater over a slope of $35°$ in a water depth of 0.330 m. The slide was modeled as a Newtonian fluid, first with parameters defined in Grilli et al. (2017), *i.e.*, a viscosity of 0.01 Pa·s and a density of 1951 kg·m^{-3}. A few other viscosity values were also tested to evaluate the sensitivity of the model. The results show that with a slide viscosity of 0.01 Pa·s, the first wave is higher than the experimental value and the wave train is not correctly reproduced on the first gauge. By reducing the viscosity, the generated waves are lower. We observe that with a viscosity of 1 Pa·s, the first wave is close
15   to the experimental results as well as the first waves in the wave train. Overall the results on wave height appears satisfactory while the slide is still slower than in the experiment.

To extrapolate these results for the La Palma computations, the following reasoning is adopted. First, it is assumed that the real slide is well represented by the granular medium used in the experiment, which may at least be considered as a better assumption than the worst case scenario considered in Abadie et al. (2012). Second, the 2D cross section of the La Palma slide
20   in Abadie et al. (2012) is $\sim$8 km^2 compared to $\sim$4 for Viroulet's slide extrapolated at real scale. As these surfaces are of the same order, the slide dynamics are assumed to be roughly similar. Third, the La Palma slide is partially submerged but with a larger subaerial portion. Because of this, the real case would be more similar to the first experiment (*i.e.*, Viroulet et al. (2014)) than to the second one (*i.e.*, Grilli et al. (2017)).

The equivalent viscosity for the real case is then obtained by scaling the optimal viscosity obtained after calibrating the
25   model against the experiments. Froude and Reynolds numbers should be the same at reduced and real scales leading to:

$$\frac{u}{\sqrt{gh}} = \frac{u'}{\sqrt{gh'}} \tag{1}$$

$$\frac{\rho u h}{\mu} = \frac{\rho u' h'}{\mu'} \tag{2}$$

where g is the acceleration of gravity, $u(u')$ a characteristic velocity, $h(h')$ a characteristic length scale and $\mu(\mu')$ the equivalent
30   viscosity at real scale (reduced scale respectively). Combining the two equations leads to:

$$\frac{\mu}{\mu'} = \sqrt{\frac{h^3}{h'^3}} \tag{3}$$

which for a viscosity $\mu' = 10$ Pa·s at reduced scale gives $\mu = 4.4 \times 10^7$ Pa·s at real scale given the length ratio. The slide considered in Abadie et al. (2012) (Figure 1) being partially submerged, the latter viscosity value is arbitrarily reduced to $\mu = 2 \times 10^7$ Pa·s to take into account of the result obtained with Grilli et al. (2017)'s experiment.

Based on these hypothesis, simulations were performed with three initial slide volumes corresponding to 20, 40 and 80 km^3, respectively (similarly as in Tehranirad et al. (2015)). The largest slide volume considered in Abadie et al. (2012), namely 450 km^3, considered very unlikely, is not considered in this paper.

2.2 Transition from Navier-Stokes to propagation models

As noted in the original THETIS simulations presented in Abadie et al. (2012), the landslide, as modeled, continues to move for a very long time (more than half an hour), but the slide local Froude number is super-critical for only a short time (less than 100 s), and it is only during this super-critical period when the resulting tsunami wave continues to grow significantly. As a result, it is not necessary to model the entire slide run-out in order to capture the generation of waves that will affect distant shorelines.

Taking the result from the THETIS model after 300 s of simulated time, once several wave fronts have already propagated away from the generation site, integrating velocity over depth, we transfer the state of the model to the Boussinesq wave model FUNWAVE-TVD (Shi et al., 2012). However, the water around the still-moving slide includes highly turbulent three-dimensional effects that cannot be represented correctly in a Boussinesq model. To remove the residual flow (that is not expected to generate significant waves) near the slide, we apply an *ad hoc* filter, as determined by numerical experimentation. It consisted in multiplying the output of THETIS (*i.e.*, free surface elevation and each velocity component) by a spatially varying function, removing the interior flow while keeping a smooth initial condition for FUNWAVE. This function is Gaussian, with a standard deviation of 15 km and the center is located at coordinates (10 km, 10 km). For more details, including validation of this approach, see Abadie et al. (2012).

After this filter is applied, local Boussinesq wave modeling is conducted on a 500-m resolution bathymetric grid taken from the Global Multi Resolution Topography (GMRT) database (Ryan et al., 2009). In order to take advantage of the fully nonlinear version of FUNWAVE-TVD, a Cartesian coordinate grid system is used. To project this onto the local area, a transverse secant Mercator projection is used (similar to the UTM system, but centered at 28.5°N and 18.5°W corresponding to +69 km, +14 km). The distortion of the entire grid is less than 1%.

After this initial phase of propagation, the results of wave elevation and horizontal velocity are transferred to larger-scale simulations to predict impact on various coastlines, as detailed below.

2.3 Models used for long distance propagation

We used four different models for the simulation of the propagation of the tsunami, each of them run by different institutions: Calypso for CEA, FUNWAVE-TVD for the BRGM, Telemac-2D for EDF and SCHISM for LARGE Laboratory. Although these models use the same basic equations, their writing may vary, as do the computation schemes. Moreover, two of the

models use Boussinesq model while the others use Non-Linear Shallow Water (NLSW) equations. These different models are detailed hereafter.

2.3.1 Calypso

Calypso is a code developed by CEA and used for tsunami propagation (Poupardin et al., 2017; Gailler et al., 2015). The model is based on NLSW equations (4, 5, 6), or Boussinesq equations (7, 8) if the area of simulation shows dispersive effects. The 2D SW equations are solved in spherical coordinates:

$$\frac{\partial h}{\partial t} + \frac{1}{\cos\theta}\left(\frac{\partial uh}{\partial\varphi} + \frac{\partial\cos\theta vh}{\partial\theta}\right) = 0 \tag{4}$$

$$\frac{\partial u}{\partial t} - fv + \frac{1}{\cos\theta}\left(u\frac{\partial u}{\partial\varphi} + \cos\theta v\frac{\partial u}{\partial\theta} - \sin\theta uv\right) = -g\frac{1}{\cos\theta}\frac{\partial\eta}{\partial\varphi} + F_\phi \tag{5}$$

$$\frac{\partial v}{\partial t} + fu + \frac{1}{\cos\theta}\left(u\frac{\partial v}{\partial\varphi} + \cos\theta v\frac{\partial v}{\partial\theta} - \sin\theta u^2\right) = -g\frac{\partial\eta}{\partial\theta} + F_\theta \tag{6}$$

where $h = \eta + d$ with η the surface elevation and d the water depth, φ and θ are the longitude and latitude, respectively, (u, v) the depth-averaged velocities along (φ, θ), f the Coriolis parameter and (F_φ, F_θ) the bottom friction force base on the Chezy formula.

In the Boussinesq equations, only the lowest-order nonlinear and dispersive terms are retained, following Pedersen and Løvholt (2008). Dispersive terms B_φ and B_θ are added to the momentum equations:

$$B_\varphi = -\frac{1}{6}\frac{d^2}{\cos^2\theta}\frac{\partial}{\partial\varphi}(\frac{\partial u_t}{\partial\varphi} + \frac{\partial(\cos\theta v_t)}{\partial\theta}) + \frac{1}{2}\frac{d}{\cos^2\theta}\frac{\partial}{\partial\varphi}(\frac{\partial hu_t}{\partial\varphi} + \frac{\partial(\cos\theta hv_t)}{\partial\theta}) \tag{7}$$

$$B_\theta = -\frac{d^2}{6}\frac{\partial}{\partial\theta}(\frac{1}{\cos\theta}\frac{\partial u_t}{\partial\varphi} + \frac{1}{\cos\theta}\frac{\partial(\cos\theta v_t)}{\partial\theta}) + \frac{d}{2}\frac{\partial}{\partial\theta}(\frac{1}{\cos\theta}\frac{\partial hu_t}{\partial\varphi} + \frac{1}{\cos\theta}\frac{\partial(\cos\theta hv_t)}{\partial\theta}) \tag{8}$$

where $u_t = \partial u/\partial t$ and $v_t = \partial v/\partial t$.

A Crank-Nicolson scheme for the temporal discretization and a finite-difference scheme for spatial derivatives are used to solve both NLSW and Boussinesq equations. For the Crank-Nicolson scheme, an iterative procedure enables the solving of the implicit set of equations. The convergence criteria is applied to the continuity equation. The spatial discretization uses centered differences for linear terms as well as for advection terms. For Boussinesq equations, the implicit momentum equations are solved by alternating implicit sweeps in the x and y components using an Alternating Direction Implicit (ADI) method. For a given direction, the dispersion terms in the other direction are discretized explicitly. For each direction (x and y), a tridiagonal system of equations is then solved at each iteration, following Pedersen and Løvholt (2008). The numerical scheme of Calypso has been described in Poupardin et al. (2018).

Four levels of nested grids are used in this computation (Figures 4 and 5). The mother grid covers Canary Islands and a large part of the Atlantic Ocean to the French coasts. It is a 2-km resolution grid with a total of 1351×1298 cells. The second grid of 1294×1404 cells covers all the French Atlantic Ocean coastline and the North of Spain with a 500-m resolution. Four grids are used to simulate the propagation of water waves in coastal regions: -the so-called "Brittany" grid covers a large region

5   in the South of Brittany with a 125-m resolution; -the "Gironde" grid covers the mouth of the Gironde estuary with a 125-m resolution; -the "Saint-Jean-de-Luz" grids with a first grid of 125-m resolution and a smaller one of 32.5-m resolution which covers the bay of Saint-Jean-de-Luz in the South West of France.

The offshore propagation is simulated by using the Boussinesq model to take into account the dispersive effects in the Atlantic Ocean. In coastal areas, the wave train is already formed and frequency dispersion may be neglected. Therefore,

10 shallow water equations are solved in the daughter grids in order to reduce the computation time.

2.3.2   FUNWAVE-TVD

FUNWAVE-TVD, run here by the BRGM group, is the most recent implementation of the Boussinesq model FUNWAVE (Wei et al., 1995), initially developed and extensively validated for nearshore wave processes, but equally used to perform tsunami case studies. The FUNWAVE-TVD code, which solves the Boussinesq equations of Chen (2006) with the adaptive vertical

15 reference level of Kennedy et al. (2001), with either fully-nonlinear equations in a Cartesian framework (Shi et al., 2012) or a weakly-nonlinear spherical coordinate formulation with Coriolis effects (Kirby et al., 2013). It uses a TVD shock-capturing algorithm with a hybrid finite-volume and finite-difference scheme to accurately simulate wave breaking and inundation by turning off dispersive terms (hence solving the NLSW equations during breaking) once wave breaking is detected (detection based on the local wave height). The code is fully parallelized using the Message Passing Interface (MPI) protocol and efficient

20 algorithms allowing a substantial acceleration of the computations with the number of cores. For operational uses, FUNWAVE-TVD has received many convenient implementations, such as the use of nested grids to refine the simulations in the interest areas, or the use of heterogeneous Manning coefficients to characterize bottom friction, the Manning coefficient is a constant $0.025 \text{ s} \cdot \text{m}^{-1/3}$.

In the framework of the U.S. NTHMP program, FUNWAVE-TVD has been validated for both tsunami propagation and

25 coastal impact, through an important set of analytical, laboratory and field benchmarks (Tehranirad et al., 2011). Other recent applications have allowed the validation of the model on real cases, such as the Tohoku-Oki tsunami (Grilli et al., 2013).

The simulation of the propagation of the tsunami to the coastlines was performed with nested grids (Figures 4 and 5) from 2.7-km resolution (Atlantic ocean) to 930 m (Antilles), 450 m (north Atlantic area), 310 m (Guadeloupe Archipelago), 110 m (Aquitaine region) and 20 m (Gironde estuary).

2.3.3   Telemac-2D

Telemac-2D is the 2D component of the Telemac-Mascaret system www.opentelemac.org. It is a finite element and a finite volume solver based on the resolution of NLSW. In this paper, it was run by the EDF group.

NLSW equations in their non-conservative form are given by:

$$\frac{\partial h}{\partial t} + div(h\boldsymbol{u}) = 0 \tag{9}$$

$$\frac{\partial u}{\partial t} + u\frac{\partial u}{\partial x} + v\frac{\partial u}{\partial y} = -g\frac{\partial \eta}{\partial x} + F_x + \frac{1}{h}div(h\mu_e grad(u)) \tag{10}$$

$$\frac{\partial v}{\partial t} + u\frac{\partial v}{\partial x} + v\frac{\partial v}{\partial y} = -g\frac{\partial \eta}{\partial y} + F_y + \frac{1}{h}div(h\mu_e grad(v)) \tag{11}$$

This non-conservative form is used for the discretization of the finite-element kernel. The conservative form is used for finite-volumes.

Telemac-2D is massively parallelized using an MPI domain decomposition approach. This feature is very useful for the

10   simulation of large problems such as the one presented here.

In this work, the mesh has 12.5 million of triangular elements and 6.4 million nodes. The limits go from the Senegal coasts in the South to the Arctic circle in the North and from the eastern American coasts to the European ones. Figure 4 shows the computational domain used with Telemac. All the boundaries are set as solid walls (note that the first wave does not reach the boundaries at the end of the simulation time).

15 **2.3.4 SCHISM**

SCHISM (Semi-implicit Cross-scale Hydroscience Integrated System Model) (Zhang et al., 2016), is a derivative product of SELFE (Zhang and Baptista, 2008a). Although the code is able to solve the 3D Reynolds Averaged Navier-Stokes equations in hydrostatic or non-hydrostatic mode, in this study only one sigma layer is used and equations are depth integrated leading to 2D NLSW equations with additional source terms for Coriolis effect, bottom friction dissipation and horizontal eddy viscosity

20   in the momentum equation such as:

$$\frac{\partial \eta}{\partial t} + \nabla.\int_{-h}^{\eta} \mathbf{u}dz = 0 \tag{12}$$

$$\frac{\partial \mathbf{u}}{\partial t} + (\mathbf{u}.\nabla)\mathbf{u} = -f \times \mathbf{u} - g\nabla\eta + \nabla.(\mu\nabla u) - \frac{\tau_{b_{(x,y)}}}{\rho(\eta+h)} \tag{13}$$

where $\mathbf{u}(x,y,t)$ is the horizontal velocity, η the free surface elevation h the mean water depth, μ the horizontal eddy viscosity, f the Coriolis factor, g the acceleration of gravity, $\tau_b = \rho\frac{g.n^2}{\sqrt[3]{H}}.U^2$ with n the Manning coefficient and $\nabla = (\frac{\partial}{\partial x}, \frac{\partial}{\partial y})$.

25   Equations 12 and 13 are solved over an unstructured mesh that covers the part of the Atlantic basin between the Canary Islands and the Lesser Antilles arc (Figure 4). The resolution is adapted to be able to accurately reproduce wave trains of

period of 12 minutes or more, with at least 20 nodes per wavelength in deep ocean. Along the coastline of interest, and for the aerial part where specific features may obstruct the water flow inland, resolution reaches 10 m. Inundation process relies on a specific inundation algorithm that is detailed and benchmarked in Zhang and Baptista (2008b). The Manning coefficient is set to 0.025 s·m$^{-1/3}$ for the whole domain. In order to avoid reflection along the domain limit, boundary conditions are set to

5 Flather type (Flather, 1976).

2.4 Locations of numerical output

In the Caribbean Sea, we detail the tsunami waves features in the vicinity of the Guadeloupe Archipelago. The latter is located 61°W and 16°N in the Lesser Antilles at 4600 km from the Cumbre Vieja Volcano. It is made up of four main groups of islands (Figure 6) with a total surface of 1628 km^2.

10   In order to compare the different models previously exposed on Europe and France, the six following synthetic gauges (Figure 7) were used: one south of Portugal and Spain to evaluate the impact in this region, one in the French abyssal plain and one in the continental shelf off the French Atlantic coast and three gauges located on the French coastline (in front of the Gulf of Morbihan, near the Gironde estuary and at the entrance of the Saint-Jean-de-Luz bay). The coordinates and depths of the six gauges are provided in Table 1.

15 ### 2.5 Run-up assessment

An accurate assessment of the actual impact of the tsunami requires refined computations on nested refined grids including local friction coefficients and an accurate knowledge of the bathymetry and the topography. In the present study, this extensive work was performed in Guadeloupe and partly in selected areas of the French Atlantic Coast (Britanny, Gironde and Saint-Jean-de-Luz) with a lower level of complexity.

20   Regarding the island of Guadeloupe, simulations were carried out with SCHISM with a refined grid of the nearshore area of about 10 m resolution along the shoreline and using variable friction coefficients dependent on the soil nature. For the submerged area, 10 classes of Manning values were used while 50 classes have been used for the aerial domain based on Corine Land Cover dataset (Büttner et al., 2004).

On the Atlantic French coast, although in the framework of the TANDEM project, high-resolution topo-bathymetry data

25 was provided in several areas in this region by the SHOM institute, the impact study was limited to preliminary computations, neglecting friction, mainly due to the relative weakness of the wave signal obtained.

To complement the results provided by simulation, we also relied on the theoretical work of Madsen and Fuhrman (2008) to make a coarse assessment of the potential hazard associated to the wave train generated with the largest slide scenario. Madsen and Fuhrman (2008) provide the following simple expressions for the maximum run-up R and the associated flow velocity V

30 generated by periodic long waves propagating over a finite slope and then a flat bottom (offshore), in terms of the similarity parameter ξ (*e.g.*, (Battjes, 1975)) and the amplitude (A_0) to depth (h_0) ratio determined at some offshore locations:

$$\frac{R}{A_0} = 2\pi^{3/4}(\frac{A_0}{h_0})^{-1/4}\xi^{-1/2} \qquad (14)$$

$$\frac{V}{\sqrt{gA_0}} = \frac{\sqrt{\pi}}{\xi}(\frac{R}{A_0})$$

(15)

$$\frac{R_{break}}{A_0} = \frac{1}{\pi}\xi^2$$

(16)

the last parameter R_{break} being a limit value for the run-up due to wave breaking.

Of course, these formula do not take into account any refraction or diffraction effects which could induce energy focusing to specific areas. Nevertheless, this methodology allows to give an idea of the damage intensity which could be caused by a given tsunami.

3 Results

3.1 Wave source computation

With a higher viscosity, the slide dynamics changes significantly compared to the inviscid case. The bulge, which was very developed in the latter case (Figure 8), is now scarcely noticeable, although it still exists (Figure 9). The slide tip is also slower ($\sim$30 m·s^{-1}, Figure 9(b)) compared to the original simulation ($\sim$100 m·s^{-1}, Figure 8). The rear part of the slide, where the velocity is maximum, is still very fast ($\sim$120 m·s^{-1}) at the initial stage of the process (Figure 9(a)) but then the maximum velocity decreases to about 50 m·s^{-1} (Figures 9(b) and (c)).

As a consequence of lower velocity and slide cross section reduction, the wave train generated is significantly less energetic (Figure 10(b)) than in the inviscid case (Figure 10(a)). After almost 10 minutes of propagation, the leading wave, which was previously about 80 m high, only reaches $\sim$30 m in the new simulation of the 80 km^3 case (Figure 10(c)). Additionally, the mean sea water level, drastically lowered at this time in the previous inviscid case, is now approximately at the initial elevation. Note that the directionality focus of the tsunami is the same in both cases with the maximum wave energy heading 20° south of West.

The wave formation is similar in sequence with the generation of a first free surface positive response reaching 400 m in the new case (compared to 800 m previously) at t=102 s, which then exhibits radial amplitude decrease and frequency dispersion (Figure 11(d)).

Of course, there is a very significant variation of wave amplitude depending on the slide volume considered (Figure 12). At t=5 min, the leading wave is $\sim$80 m high in the largest slide volume scenario (*i.e.*, 80 km^3) and is only 50 m and 20 m for smaller slide volumes (40 and 20 km^3, respectively).

3.2 Filtered solution

Taking the THETIS solution (Figure 12) after the initial 5 minutes of propagation, and applying the filter described in Section 2.2, the subsequent wave propagation is simulated with the Boussinesq wave model FUNWAVE-TVD with a 500 m grid for an additional 15 minutes, which is sufficient to consider the interaction between the tsunami and the nearby islands.

5   The effect of the filtering can be seen clearly in Figure 13, where flow near La Palma is strongly damped, but the leading waves are unaffected. As shown by Abadie et al. (2012), this has been found to represent the first several wave fronts, and better represent the overall wave field, as compared to an unfiltered solution.

The resulting wave elevation and velocity fields (*e.g.*, Figure 14) can then be transferred to models with larger grids for predicting impact on the distant coastlines. The effect of dispersion, due to the large depth (relative to the wavelength) and the

10   interaction with nearby islands is evident in the results.

3.3 Wave features by regions

Figure 15 shows the maximal simulated sea surface elevation for the 80 km^3 scenario computed by FUNWAVE-TVD (the picture is very similar for the other codes Calypso and Telemac-2D) at an oceanic scale, from the source to the studied areas. A gradual decrease of the maximum wave height due to radial attenuation can be observed, modulated by energy focusing in

15   narrow directions.

3.3.1 Near the generation area

Territories close to the generation area are highly affected. The first locations impacted are the other surrounded Canary Islands, nearby archipelagos (Madeira Island, Cape Verde) and west Africa, especially western Sahara (Dakhla city - 100000 inhabitants) and specific parts of Morocco by refraction on shallower part of the local bathymetry (Agadir, Essaouira, Safi -

20   800000 inhabitants overall). In the latter areas, the waves are larger than 5 m.

3.3.2 In the Caribbean Sea - Guadeloupe Archipelago (SCHISM model)

A detailed investigation of simulation results shows that the eastern Caribbean is located on an energy focusing path and, as a result, is among the most exposed areas in the far field, as suggested by Gisler et al. (2006). The wave train arriving around the Guadeloupe Archipelago is composed of a main first wave about 2 to 3 m high and 80 to 100 km long (Figure 16).

25   In Figure 17, the maximum surface elevation distribution shows that the main exposed areas are Marie Galante, Les Saintes, La Désirade and Saint-François. Waves are shoaling over the shelf out of Saint-François and focus a large amount of the energy toward Saint-François, La Désirade and to a lesser extent in Sainte-Anne (between Le Gosier and Saint-François). Maximum wave height distribution display the same patterns whatever the slide volume and differs only in wave amplitude. Arrival times and wave heights are shown on Figure 18 for the four stations located on Figure 6. The Eastern parts, Le Moule and

30   La Désirade, are first exposed to the incoming wave front, respectively 5 h 48 min and 5 h 57 min after the volcano collapse event. Then the southern coasts are impacted as the wave wraps around Grande Terre. Le Gosier is hit after 6 h 10 min, the

time difference between the easterly point and the leeward side being about 15 min. Wave heights can reach up to 5 m at La Desirade for the largest slide volume, 3-4 m in Le Gosier and Le Moule and ∼2 m in the more sheltered so-called Bouillante location. The wave period is about 12 minutes on the three first locations and seems to shorten to about 6 minutes on the lee side of the island.

5   A comparison between SCHISM and FUNWAVE-TVD is given in Figure 19. Time arrival is quite consistent between the two models after almost 6 hours of travel. The overall wave trains and the computed wave amplitudes are comparable even though not negligible differences can be observed.

3.3.3   Europe and France

The wave propagating toward Europe is obviously less energetic than in the western direction on which the main part of the

10   energy is focused (Figure 15). Nevertheless, Portugal, the western coast of Spain and to a lesser extent, the southern coasts of Ireland and England are significantly affected. Lisbon, Porto, Vigo and Corunna appear to be the main cities at risk for the 80 km^3 tsunami scenario with a tsunami amplitude of about 2 m.

    Overall, the coasts of France are protected by the Iberian Peninsula (Figure 15 - right panel). When approaching the French Atlantic coastline, the wave experiences shoaling on the continental shelf and the wave height slightly increases. In the Calypso

15   simulation, the wave train striking the Atlantic coast of France (Figure 20) is composed of several waves between 0.3 and 0.5 m of amplitude and about 50 km of wavelength. Note that higher frequency components, superimposed on the main wave signal, make this estimation only very qualitative.

    The analysis of the different gauges (Figures 21, 22, 23, 24) shows that the wave forms computed by the three models used in this area (*i.e.*, Calypso, FUNWAVE-TWD and Telemac-2D) shows similarities (*i.e.*, the first wave) but also significant

20   discrepancies (*i.e.*, the amplitude of the trailing waves). In average, the first wave amplitude reaches between 65 and 75 cm at Gauge 1 between the South of Portugal and the North of Morocco (Figure 21 (A)) and around 15 cm at Gauge 2 (Figure 21 (B)) in the abyssal plain of the Bay of Biscay for the 80 km^3 slide scenario. The wave height of the leading wave is drastically reduced for the 20 km^3 slide scenario (Figure 22 (A)), reaching approximately 13 cm at Gauge 1 and only 3 cm at Gauge 2 (Figure 22 (B)). These results are approximately consistent with a r^{-1} propagation attenuation. Based on the signal

25   recorded at Gauges 1 and 2, the leading positive wave also seems to experience an increase of period, from 7.5 minutes to 13 minutes approximately (only counting the positive signal), independently of the slide scenario. This apparent period increase is associated to the wave low frequency component which progressively appears more and more important in the signal.

    Gauge 3 is located right after on the beginning of the continental shelf. The increase of wave height is not very significant compared to Gauge 2 (Figures 23 (A) and 24 (A)).

30   Since the transition between the abyssal plain and the continental shelf is quite abrupt and due to the large wavelength, the increase of the wave height is not significant. For the 80 km^3 scenario, the height of the wave is between 15 and 20 cm on the continental shelf (Figure 23 (A)), between 30 and 40 cm in south Brittany (Figure 23 (B)), between 15 and 25 cm in the Gironde estuary (Figure 23 (C)), and between 30 and 40 cm in Saint-Jean-de-Luz (Figure 23 (D)). The leading wave on Figures 23 (A) to (D) reaches the gauges after 3 h 20 min (or 3 h 25 min since the landslide triggering), 4 h 10 min, 4 h 35 min and 3 h

40 min of propagation, respectively. At this time, the main period of the wave is difficult to assess as it is a mix of low and high frequencies. Taking only the low frequency components, the wave exhibits periods of 30 minutes in the two gauges located norther and 60 minutes for the two gauges located more in the South. Note that we observe a lag time of 5 to 10 minutes of the arrival times between the two slide scenarios.

5   Figure 24 (A) shows that for the 20 km^3 scenario, the waves are one order of magnitude smaller (between 1 and 6 cm) and show lower periods.

3.4   Run-up

3.4.1   Analytical run-up formula - France and Guadeloupe

To assess run-up and maximum flow velocity along the French Atlantic coastline, Gauge 3 of Figure 7 is considered. The

10   average depth h_0 around this location is about 100 m and the tsunami amplitude A_0, 0.2 m. To assess the possible range for the surf similarity parameter, wave periods and beach slopes are needed. Several wave periods can be considered in Figure 23 (A). Among the latter, a low frequency wave of about 36 minute period and a higher frequency wave of about 6 min period are particularly present in this plot. As for beach slopes, values between 1/100 and 1/10 can be found along the french Atlantic coast. Those parameters give rise to a very large range for the surf similarity parameter ξ (*i.e.*, from 1.5 to 30) covering the

15   whole spectrum of possible run-up scenario.

Run-up and maximum flow velocities are plotted in Figure 25 using Equations 14, 15 and 16. The run-up plot displays two distinctive parts with respect with the maximum value. On the left hand side, the run-up is limited due to wave breaking (*i.e.*, $R > R_{break}$) whereas on the right hand side, it is not. The same holds for the flow velocity plot. This figure shows that the run-up should be everywhere less than 2 m and the associated flow velocity less than about 3 m·s^{-1}. The largest run-up occurs

20   for ξ around 6-7, therefore for instance on beaches involving a 1/50 slope and considering the 36 min period. This slope is a common value in the Aquitaine region. Nevertheless, the quite moderate values of the run-up in this less favorable case show that the consequences of such event may stay limited for this portion of the coast. Note that the conclusion is not the same for the coast of Portugal, as the latter may experience a maximum run-up of 6 m (average value 3 m) and a maximum flow velocity of 8 m·s^{-1} (resp. 1.5 m·s^{-1}) based on the tsunami estimation at Gauge 1 (A_0=0.7 m and h_0=300 m).

25   Run-up on the Guadeloupe Archipelago can also be assessed based on the same procedure. First, wave characteristics are evaluated considering the wave field plotted on Figure 16. On the left panel of this figure, the water depth is about 2000 m, the wave amplitude about 1.5 m and the wave length about 100 km. With those values, ξ is found to vary between about 2 to 40 for slopes from 1/80 to 1/6, respectively, which are the mean slope values range encountered around the Guadeloupe. The plot of Figure 26 allows to assess the expected run-up and maximum velocity for the Guadeloupe area. The results show that the

30   impact may be dramatic with run-up in the range 10 to 18m and velocities of the order of $6 - 12\ m/s$ for common ξ values.

3.4.2 Numerical simulation of flooding - examples in France (Calypso model) and Guadeloupe (SCHISM model)

For the French Atlantic coast area, results obtained can only be considered as very preliminary results due to the model resolution considered (32.5 m for Saint-Jean-de-Luz and 125 m for Le Morbihan and Gironde). In Saint-Jean-de-Luz the run-up appears very limited due to the small amplitude wave obtained in this area. The incident wave is more energetic off the coast

5 of Brittany. In this area, due to energy focusing, run-up may reach 2 to 3 m as illustrated in Figure 27.

In Guadeloupe, the impact of the 80 km^3 is very significant as illustrated on the inundation maps provided on Figure 28. The flood penetration inland, not uniform as depending on the specific local topography, is nevertheless almost everywhere on the order of 500 m to 1 km. It can be noted that the extreme values of run-up predicted by the analytical run-up formula are not reached in these plots, first due to the friction coefficient used in the model, whose value and distribution drastically influence

10 the inundation pattern, and second, the slopes of these specific areas, which correspond to large ξ values.

4 Discussion

The main goal of the present study was to improve the state of the art for the potential La Palma tsunami source and to use this new proposed scenario to perform a risk assessment for Europe and particularly for French territories. Such low occurrence frequency and high magnitude sources are particularly important to study as accurately as possible since, due to the difficulty

15 to assess their precise probability, they often serve as reference for hazard mitigation study (Tehranirad et al., 2015).

The first result of the present work is the new tsunami source computed by Navier-Stokes simulation (for the initial 5 minutes), *ad hoc* filtering and Boussinesq propagation (for the following 15 minutes). As stressed previously, this source is more realistic than that considered in Abadie et al. (2012) due to the much larger viscosity used which is assumed to better approximate a granular slide. To support this, a comparison with existing granular experiments was performed and

20 the results extrapolated at real scale using a Froude/Reynolds similitude. Based on this new computation, we observed a significant diminution of the initial wave compared to the first assessment proposed in Abadie et al. (2012) (*i.e.*, wave height approximately half that of previously computed after 10 minutes of propagation for the 80 km³ scenario). The new source (after filtering and propagation in the Boussinesq model) is made available through the SEANOE (SEA scieNtific Open data Edition) portal Abadie et al. (2019).

25 The second result is a presumably better hazard assessment in Europe generally, and a new detailed hazard assessment for France and Guadeloupe. Considering a credible yet extreme 80 km³ scenario, it is shown that the impact on the French Atlantic coast would remain moderate, but could also be significant on the coast of Portugal and be very significant in the Guadeloupe Archipelago. A direct comparison with Tehranirad et al. (2015) is difficult as the areas of interest were not the same in the two papers. Nevertheless, for instance, Tehranirad et al. (2015) found waves up to 10 m in the vicinity of Western Sahara, and 5 m

30 waves on the Portuguese coast while they respectively reach 5 m and about 2 m in the present work, so the decrease is clear also far from the source.

An additional product of the study is the comparison between several numerical models in regions of overlapping interest, either based on dispersive or non-dispersive set of equations. While more complete benchmarks are considered within inter-

national or national project such as NTHMP (Horrillo et al., 2015) or the present TANDEM project, this comparison on a large-scale problem is able to provide some interesting physical insight. Tsunamis are generally considered as non-dispersive waves which can be satisfactorily approximated by the NLSW equations. Nevertheless, this assumption is often not valid for tsunami generated by landslide (e.g.,Mader (2001)), due to the much shorter wavelength. In the case of the La Palma collapse

5   scenario, Gisler et al. (2006) and Løvholt et al. (2008) emphasized the importance of the dispersive effects, even in the far-field.

In the present study, recall that FUNWAVE-TVD is dispersive, Calypso included dispersive effects for the offshore propagation but not in the nearshore areas, whereas SCHISM and Telemac-2D were run in a non-dispersive manner. In the comparison performed in the present paper, the different models generally produce consistent results especially regarding prediction of the tsunami time of arrival and first wave amplitude. The rest of the wave field is often more problematic, and normally when

10   this seen, it can be attributed to the dispersive trailing waves. Indeed, on all the synthetic gauges analyzed in Europe and France (e.g., Figure 21), high frequency waves are visible, particularly for the Calypso signal and in a lesser extent for the FUNWAVE-TVD signal. A closer look suggests that generally the differences are due only to resolution. Figure 29 shows the water wave elevations comparison between Calypso and FUNWAVE-TVD at Gauge 5 (near the Gironde estuary) for different resolutions: 2 and 2.7 km (Figure 29(A)), 500 and 450 m (Figure 29(B)), 125 and 110 m (Figure 29(C)), respectively. Noting

15   that the depth is only 10 m (Table 1), a linear wave of period 10 minutes would have a wavelength around 6 km. Therefore the "high-frequency" trailing waves therefore do not appear to be a numerical instability or a question of irregularities in model bathymetry, but simply a question of model resolution. As the model resolution is increased for both Calypso and FUNWAVE-TVD, considering the first hour after the first wave impact, which is often most important (neglecting local resonances along the coastline), the two models converge to the same solution.

20   Hence, if we omit the problem of high frequency waves, the results are consistent among the different models. This may signify that the 15 minutes of Boussinesq model propagation at the beginning of the simulation, which was provided to all models, is actually sufficient to take into account the eventual dispersive effects and allowed the NLSW models to produce a satisfactory solution after propagation. This can be illustrated by the tsunami amplitude decay rate obtained by these models after a transoceanic propagation. For instance, Figure 30) shows amplitude decay for the 40 km^3 case along the transect

25   presented on Figure 4 during the transoceanic travel for the SCHISM model. The rate of decay seems to be between $r^{-0.69}$ and $r^{-0.72}$, depending on the method considered, and can be compared the values of $r^{-0.82}$ given in Løvholt et al. (2008).

Of course there are some limitations in this study which may provide the basis for future improvements. Hence, as pointed out by Wynn and Masson (2003), past debris avalanches in the Canary Islands may have occurred in a retrogressive way, and whether the flank collapse occurs en masse or in successive stages is crucial in terms of wave generation. The present work did

30   not explicitly take into account this possibility. Nevertheless, we proposed several slide volume scenarios which can be used for a crude assessment of the wave reduction in case of a retrogressive process. For instance, the 20 km^3 scenario may give an idea of what would happen if a 80 km^3 slide were occurring progressively or in sequence. But the interaction between the successive slides are by no means studied here and is left for future research.

5 Conclusions

The wave generated by a potential Cumbre Vieja volcano flank collapse and its impact in Europe, France and Guadeloupe was studied in this work. The source computation used an improved characterization of the slide rheology compared to previous works. Moreover, the subsequent propagation was performed using different models which allows for a model comparison on a real configuration. The main conclusions of the work performed are the following:

- The new wave source is reduced in half compared to previous estimations mainly due to the improved rheology calibration.

- The wave impact is still very significant on nearby areas, or on more remote coasts but located on the path of the maximum wave energy for the maximum slide volume considered here (i.e., 80 km^3). Smaller slide volumes (i.e., 40 km^3 and 20 km^3) would have more moderate impacts on these remote areas.

- In Europe, the impact may be considered as moderate to significant in the most exposed areas such as some areas in Portugal and Spain and weak to moderate along the French Atlantic coast.

- This work allowed for a view of the differences between four different models used for propagation (Calypso, FUNWAVE-TVD, Telemac-2D and SCHISM) for overlapping regions of interest. The four codes tested are in general agreement with each others, except for the appearance of high frequency waves in the signal at the highest resolution.

- Finally, computational results do not show large differences in the first or maximum wave amplitude when comparing NLSW non-dispersive and dispersive models, likely due to the initial common Boussinesq modeling ensuring the correct accounting of dispersion at the generation site for at least the first waves. In addition, the continental shelf of Europe is not as wide as along North America where the impact was previously studied, and where dispersive effects can more clearly be seen.

Data availability. The new calibrated source (after filtering and propagation in the Boussinesq model) for the La Palma tsunami is made available through the SEANOE (SEA scieNtific Open data Edition) portal Abadie et al. (2019).

Acknowledgements. This work has been performed in the framework of the PIA RSNR French program TANDEM (Grant no: ANR-11-RSNR-00023-01) and as a part of the project C3AF, funded by the ERDF and the Region Guadeloupe. Part of this work was supported by the LRC Yves Rocard (Laboratoire de Recherche Conventionné CEA-ENS).

References

Abadie, S., Morichon, D., Grilli, S., and Glockner, S.: Numerical simulation of waves generated by landslides using a multiple-fluid Navier-Stokes model, Coastal engineering, 57, 779–794, 2010.

Abadie, S., Harris, J. C., Grilli, S. T., and Fabre, R.: Numerical modeling of tsunami waves generated by the flank collapse of the
5   Cumbre Vieja Volcano (La Palma, Canary Islands): Tsunami source and near field effects, Journal of Geophysical Research, 117, https://doi.org/10.1029/2011JC007646, http://www.agu.org/pubs/crossref/2012/2011JC007646.shtml, 2012.

Abadie, S., Paris, A., Ata, R., Roy, S. L., Arnaud, G., Poupardin, A., Clous, L., Heinrich, P., Harris, J., Pederos, R., and Krien, Y.: La Palma landslide tsunami: computation of the tsunami source with a calibrated multi-fluid Navier-Stokes model and wave impact assessment with propagation models of different types, SEANOE, 2019.

10 Athukorala, P.-c. and Resosudarmo, B. P.: The Indian Ocean tsunami: Economic impact, disaster management, and lessons, Asian Economic Papers, 4, 1–39, 2005.

Battjes, J. A.: Surf similarity, in: Coastal Engineering 1974, pp. 466–480, 1975.

Büttner, G., Feranec, J., Jaffrain, G., Mari, L., Maucha, G., and Soukup, T.: The CORINE land cover 2000 project, EARSeL eProceedings, 3, 331–346, 2004.

15 Chen, Q.: Fully nonlinear Boussinesq-type equations for waves and currents over porous beds, Journal of Engineering Mechanics, 132, 220–230, 2006.

Clous, L. and Abadie, S.: Simulation of energy transfers in waves generated by granular slides, Landslides, https://doi.org/10.1007/s10346-019-01180-0, https://doi.org/10.1007/s10346-019-01180-0, 2019.

Elsworth, D. and Day, S. J.: Flank collapse triggered by intrusion: the Canarian and Cape Verde Archipelagoes, Journal of Volcanology and
20 Geothermal Research, 94, 323–340, 1999.

Flather, R.: A tidal model of the northwest European continental shelf, Mem. Soc. Roy. Sci. Liege, 10, 141–164, 1976.

Gailler, A., Calais, E., Hébert, H., Roy, C., and Okal, E.: Tsunami scenarios and hazard assessment along the northern coast of Haiti, Geophysical Journal International, 203, 2287–2302, 2015.

Gisler, G., Weaver, R., and Gittings, M. L.: SAGE calculations of the tsunami threat from La Palma, Sci. Tsunami Hazards, 24, 288–312,
25 2006.

Grilli, S. T., Harris, J. C., Bakhsh, T. S. T., Masterlark, T. L., Kyriakopoulos, C., Kirby, J. T., and Shi, F.: Numerical simulation of the 2011 Tohoku tsunami based on a new transient FEM co-seismic source: Comparison to far-and near-field observations, Pure and Applied Geophysics, 170, 1333–1359, 2013.

Grilli, S. T., Shelby, M., Kimmoun, O., Dupont, G., Nicolsky, D., Ma, G., Kirby, J. T., and Shi, F.: Modeling coastal tsunami hazard from
30 submarine mass failures: effect of slide rheology, experimental validation, and case studies off the US East Coast, Natural Hazards, 86, 353–391, 2017.

Hebert, H.: the TANDEM project Team, 2014, Project TANDEM (Tsunamis in the Atlantic and the English ChaNnel: Definition of the Effects through numerical Modeling)(2014-2018): a French initiative to draw lessons from the Tohoku-oki tsunami on French coastal nuclear facilities, EGU, 2014.

35 Horrillo, J., Grilli, S. T., Nicolsky, D., Roeber, V., and Zhang, J.: Performance benchmarking tsunami models for NTHMP's inundation mapping activities, Pure and Applied Geophysics, 172, 869–884, 2015.

Jop, P., Forterre, Y., and Pouliquen, O.: A constitutive law for dense granular flows, Nature, 441, 727, 2006.

Kennedy, A. B., Kirby, J. T., Chen, Q., and Dalrymple, R. A.: Boussinesq-type equations with improved nonlinear performance, Wave Motion, 33, 225–243, 2001.

Kirby, J. T., Shi, F., Tehranirad, B., Harris, J. C., and Grilli, S. T.: Dispersive tsunami waves in the ocean: Model equations and sensitivity to dispersion and Coriolis effects, Ocean Modelling, 62, 39–55, 2013.

5 Lagrée, P.-Y., Staron, L., and Popinet, S.: The granular column collapse as a continuum: validity of a two-dimensional Navier–Stokes model with a μ(I)-rheology, Journal of Fluid Mechanics, 686, 378–408, 2011.

Løvholt, F., Pedersen, G., and Gisler, G.: Oceanic propagation of a potential tsunami from the La Palma Island, Journal of Geophysical Research: Oceans, 113, 2008.

Mader, C. L.: Modeling the La Palma landslide tsunami, Science of Tsunami Hazards, 19, 150–170, 2001.

10 Madsen, P. A. and Fuhrman, D. R.: Run-up of tsunamis and long waves in terms of surf-similarity, Coastal Engineering, 55, 209–223, 2008.

Masson, D., Watts, A., Gee, M., Urgeles, R., Mitchell, N., Le Bas, T., and Canals, M.: Slope failures on the flanks of the western Canary Islands, Earth-Science Reviews, 57, 1–35, 2002.

Mikami, T., Shibayama, T., Esteban, M., and Matsumaru, R.: Field survey of the 2011 Tohoku earthquake and tsunami in Miyagi and Fukushima prefectures, Coastal Engineering Journal, 54, 1250 011–1, 2012.

15 Pararas-Carayannis, G.: Evaluation of the threat of mega tsunami generation from postulated massive slope failures of island stratovolcanoes on La Palma, Canary Islands, and on the island of Hawaii, Science of Tsunami Hazards, 20, 251–277, 2002.

Paris, R., Ramalho, R. S., Madeira, J., Ávila, S., May, S. M., Rixhon, G., Engel, M., Brückner, H., Herzog, M., Schukraft, G., et al.: Mega-tsunami conglomerates and flank collapses of ocean island volcanoes, Marine Geology, 395, 168–187, 2018.

Pedersen, G. and Løvholt, F.: Documentation of a global Boussinesq solver, Tech. rep., Department of Mathematics, University of Oslo,
20 Norway, 2008.

Popinet, S.: Gerris: a tree-based adaptive solver for the incompressible Euler equations in complex geometries, Journal of Computational Physics, 190, 572–600, 2003.

Poupardin, A., Heinrich, P., Frère, A., Imbert, D., Hébert, H., and Flouzat, M.: The 1979 submarine landslide-generated tsunami in Mururoa, French Polynesia, Pure and Applied Geophysics, 174, 3293–3311, 2017.

25 Poupardin, A., Heinrich, P., Hébert, H., Schindelé, F., Jamelot, A., and Reymond, D.: Traveltime delay relative to the maximum energy of the wave train for dispersive tsunamis propagating across the Pacific Ocean: the case of 2010 and 2015 Chilean Tsunamis, Geophysical Journal International, 214, 1538–1555, 2018.

Ryan, W. B. F., Carbotte, S. M., Coplan, J. O., O'Hara, S., Melkonian, A., Arko, R., Weissel, R. A., Ferrini, V., Goodwillie, A., Nitsche, F., Bonczkowski, J., and Zemsky, R.: Global Multi-Resolution Topography synthesis, Geochemistry, Geophysics, Geosystems, 10,
30 https://doi.org/10.1029/2008GC002332, http://dx.doi.org/10.1029/2008GC002332, q03014, 2009.

Shi, F., Kirby, J. T., Harris, J. C., Geiman, J. D., and Grilli, S. T.: A high-order adaptive time-stepping TVD solver for Boussinesq modeling of breaking waves and coastal inundation, Ocean Modelling, 43-44, 36–51, 2012.

Tappin, D., Grilli, S., Ward, S., Day, S., Grilli, A., Carey, S., Watt, S., Engwell, S., and Muslim, M.: The devastating eruption tsunami of Anak Krakatau - 22nd December 2018, in: EGU General Assembly Conference Abstracts, vol. 21 of *EGU General Assembly Conference*
35 *Abstracts*, p. 18326, 2019.

Tehranirad, B., Shi, F., Kirby, J., Harris, J., and Grilli, S.: Tsunami benchmark results for fully nonlinear Boussinesq wave model FUNWAVE-TVD, Tech. rep., Version 1.0. Technical report, No. CACR-11-02, Center for Applied Coastal Research, University of Delaware, 2011.

Tehranirad, B., Harris, J. C., Grilli, A. R., Grilli, S. T., Abadie, S., Kirby, J. T., and Shi, F.: Far-Field Tsunami Impact in the North Atlantic Basin from Large Scale Flank Collapses of the Cumbre Vieja Volcano, La Palma, Pure and Applied Geophysics, 172, pp 3589–3616, https://doi.org/10.1007/s00024-015-1135-5, http://link.springer.com/10.1007/s00024-015-1135-5, 2015.

Viroulet, S., Sauret, A., Kimmoun, O., and Kharif, C.: Granular collapse into water: toward tsunami landslides, Journal of visualization, 16, 189–191, 2013.

Viroulet, S., Sauret, A., and Kimmoun, O.: Tsunami generated by a granular collapse down a rough inclined plane, EPL (Europhysics Letters), 105, 34 004, 2014.

Ward, S. N. and Day, S.: Cumbre Vieja volcano—potential collapse and tsunami at La Palma, Canary Islands, Geophysical Research Letters, 28, 3397–3400, 2001.

Wei, G., Kirby, J. T., Grilli, S. T., and Subramanya, R.: A fully nonlinear Boussinesq model for surface waves. Part 1. Highly nonlinear unsteady waves, Journal of Fluid Mechanics, 294, 71–92, 1995.

Wynn, R. and Masson, D.: Canary Islands landslides and tsunami generation: Can we use turbidite deposits to interpret landslide processes?, in: Submarine mass movements and their consequences, pp. 325–332, Springer, 2003.

Zhang, Y. and Baptista, A. M.: SELFE: a semi-implicit Eulerian–Lagrangian finite-element model for cross-scale ocean circulation, Ocean modelling, 21, 71–96, 2008a.

Zhang, Y. J. and Baptista, A. M.: An efficient and robust tsunami model on unstructured grids. Part I: Inundation benchmarks, Pure and Applied Geophysics, 165, 2229–2248, 2008b.

Zhang, Y. J., Ye, F., Stanev, E. V., and Grashorn, S.: Seamless cross-scale modeling with SCHISM, Ocean Modelling, 102, 64–81, 2016.
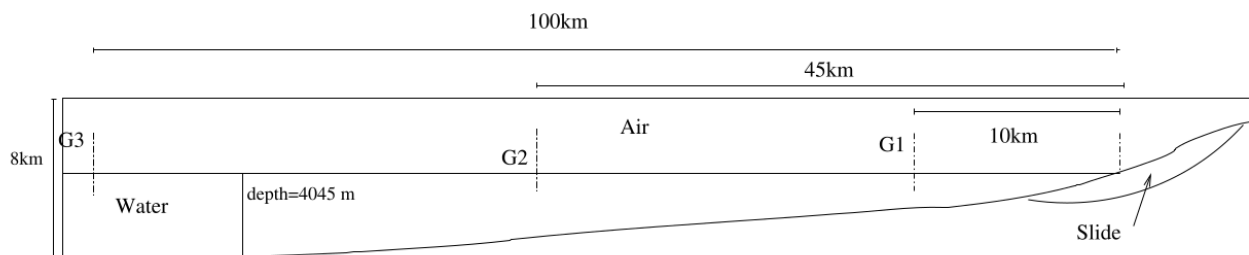
Figure 1. Cross section of the 80 km^3 La Palma slide scenario considered in Abadie et al. (2012).
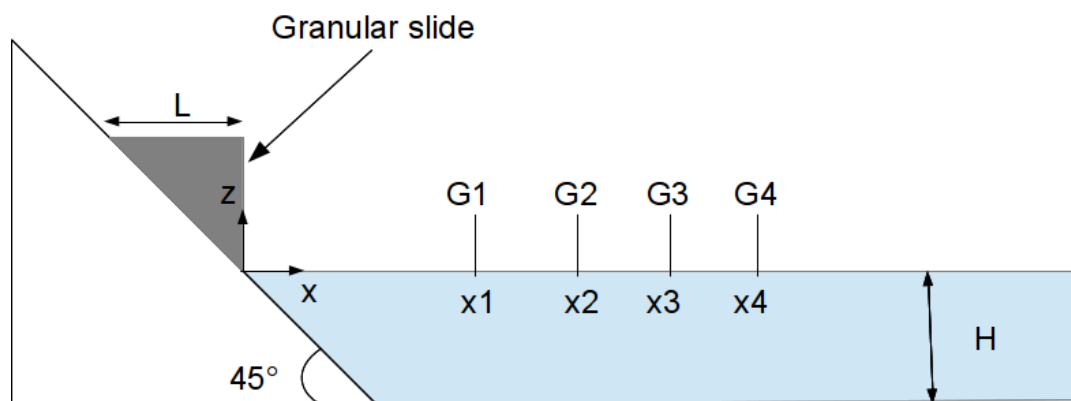
Figure 2. Sketch of the experiment performed in Viroulet et al. (2014).
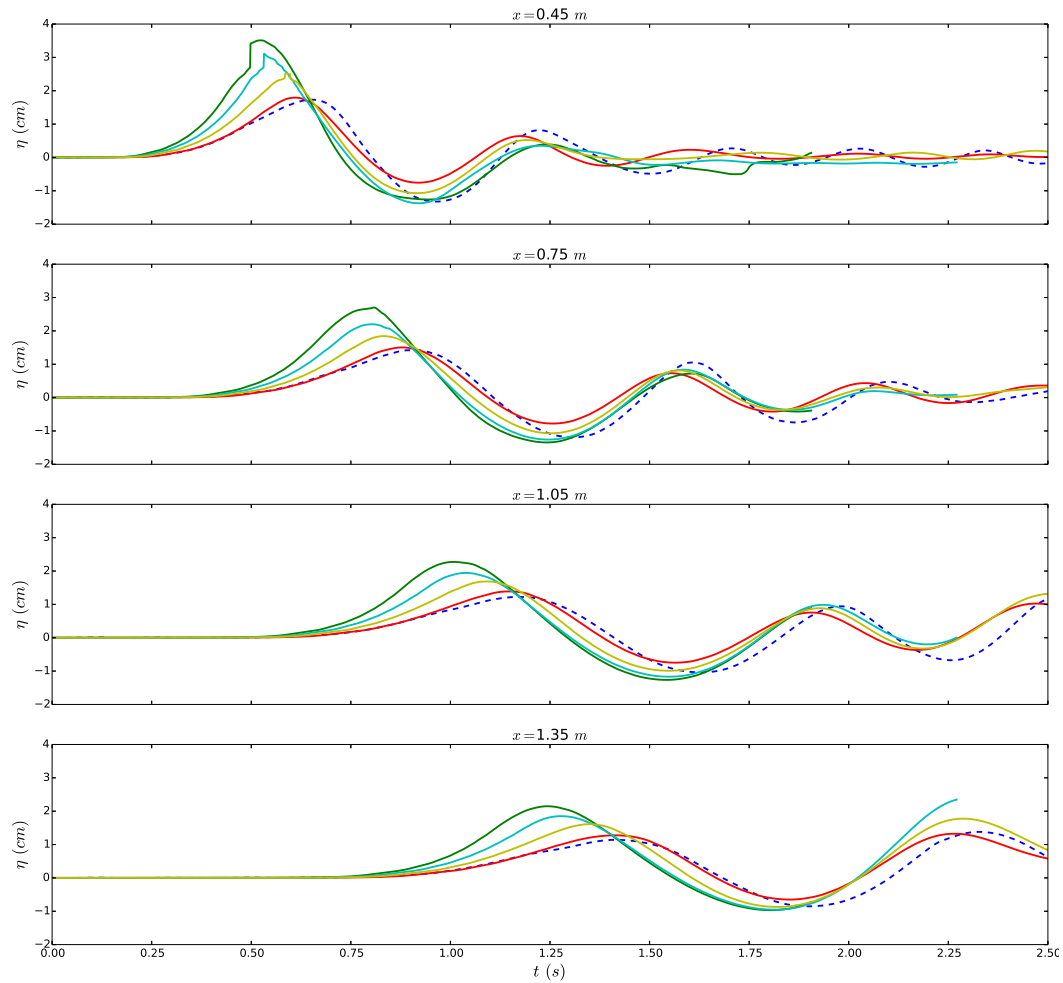
Figure 3. Free-surface elevation at the gauges for the experiment (blue discontinuous line) and the simulations for different values of viscosity, η=1 Pa·s: green line, η=2 Pa·s: cyan line, η=5 Pa·s: yellow line and η=10 Pa·s: red line; 0.1 s between two figures.
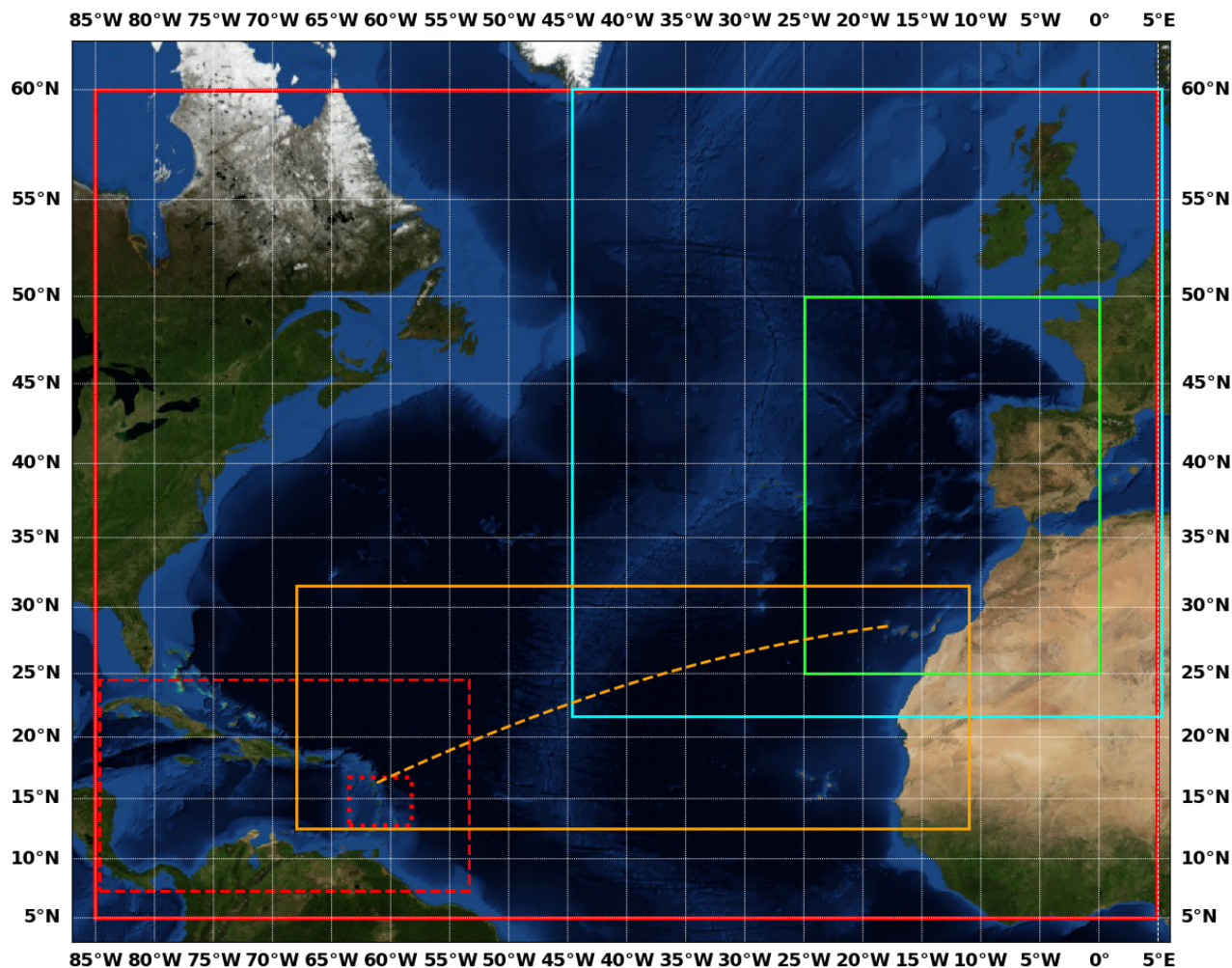
Figure 4. Computational domains for Calypso (2-km resolution in solid green), FUNWAVE-TVD (2.7 km in solid red, 930 m in dashed red and 310 m in dotted red), Telemac-2D (solid blue; variable resolution) and SCHISM (solid orange; variable resolution). The dashed orange curve represents the transect between the source and the Guadeloupe Archipelago.
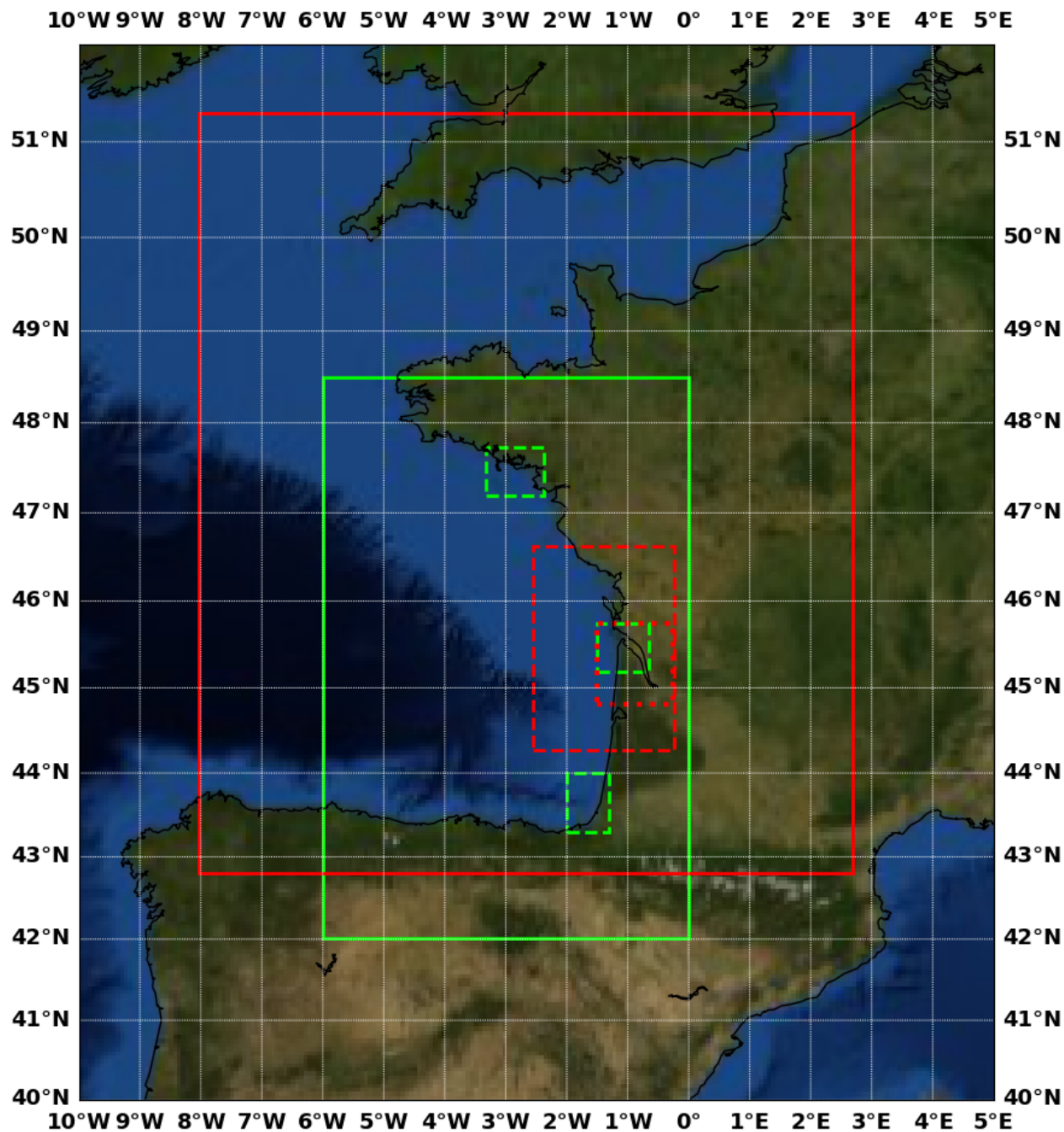
Figure 5. Computational domains for Calypso (500-m resolution in solid green, 32.5 or 125 m in dashed green) and FUNWAVE-TVD (450 m in solid red, 110 m in dashed red and 20 m in dotted red).
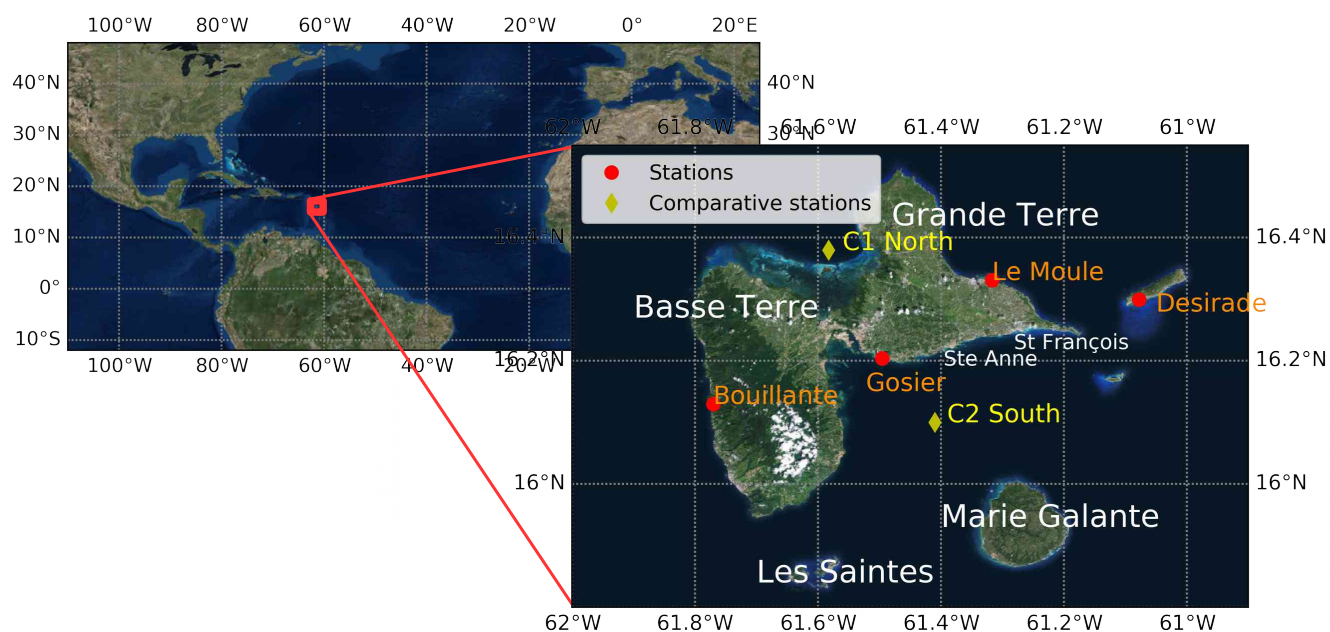
Figure 6. Guadeloupe Archipelago and locations of the wave gauges. World Imagery Map source credits: Esri, DigitalGlobe, GeoEye, i-cubed, Earthstar Geographics, CNES/Airbus DS, USDA, USGS, AEX, Getmapping, Aerogrid, IGN, IGP, swisstopo, and the GIS User Community.

![Map showing the location of six gauges in the North Atlantic near the Iberian Peninsula and northwest Africa, with points numbered 1–6 and a Source point marked.]
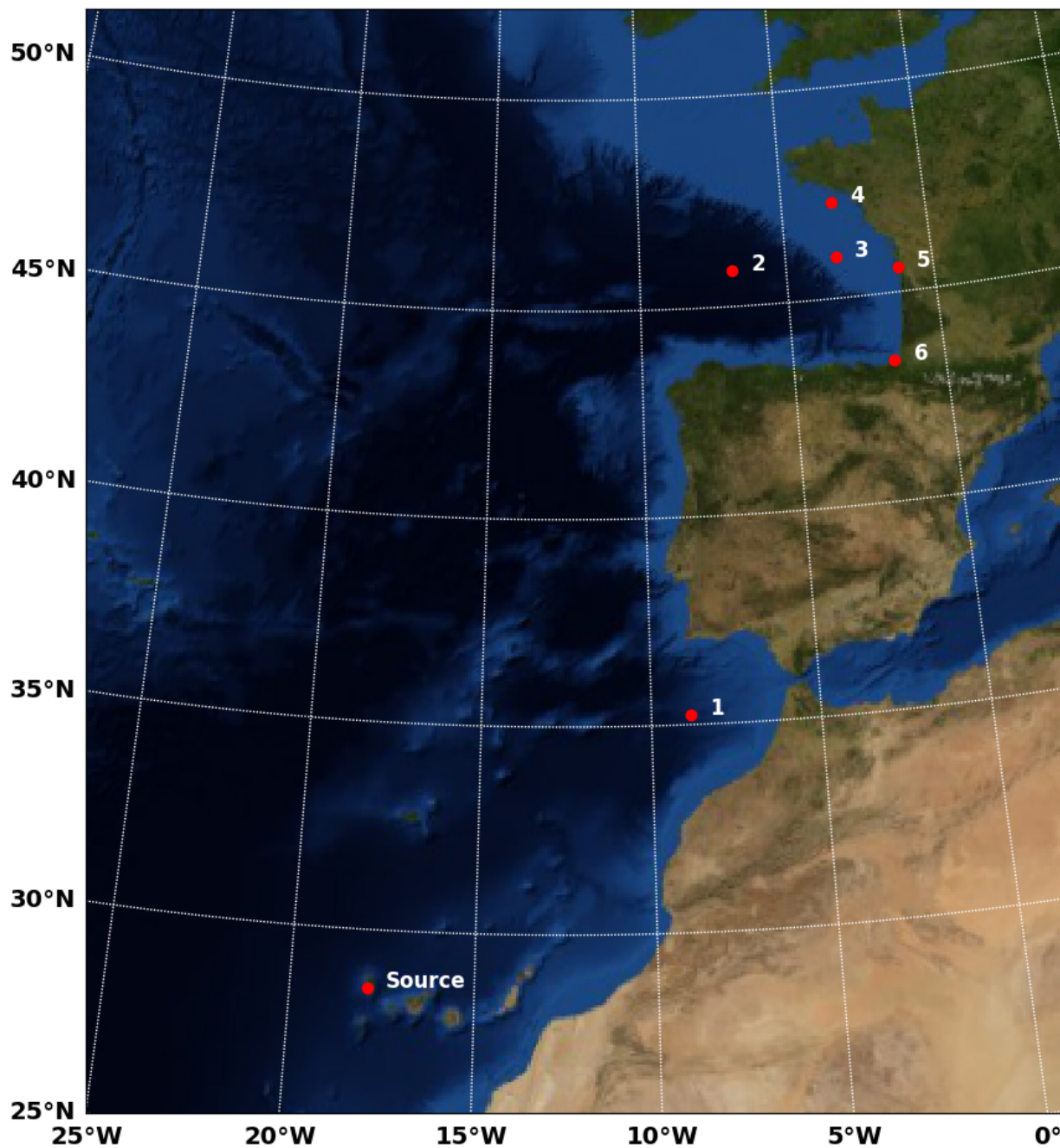
Figure 7. Location of the six gauges used to compare the simulations of Calypso, FUNWAVE and Telemac-2D.
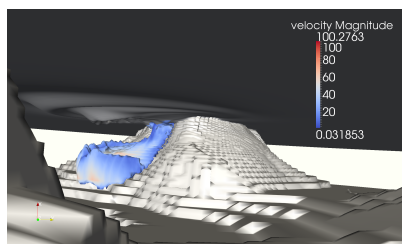
Figure 8. Snapshot of 0.1 slide volume fraction contour colored by velocity magnitude at t=250 s with inviscid slide (Abadie et al. (2012)).

(a)   (b)   (c)
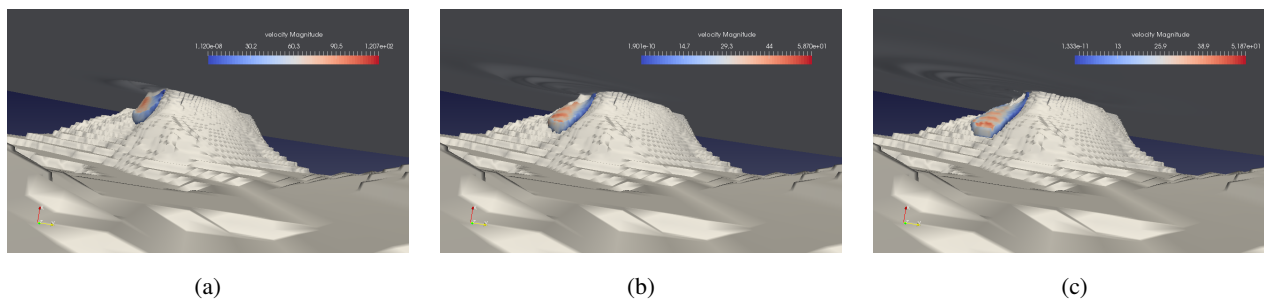
Figure 9. THETIS 3D computations for 80 km^3 slide volume. Snapshots of 0.1 slide volume fraction contour colored by velocity magnitude, at (a): t=102 s, (b): 230 s and (c): 342 s. Slide viscosity 2×10^7 Pa·s.

(a)   (b)   (c)
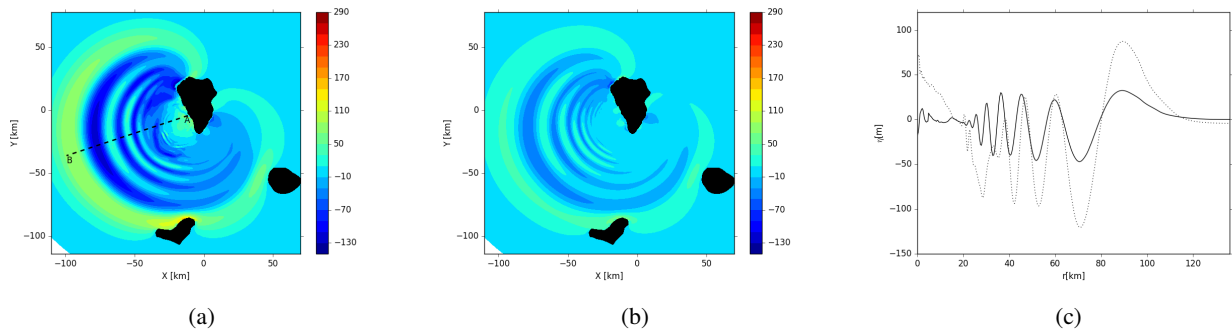
Figure 10. THETIS 3D computations for the 80 km^3 slide scenario, $t \approx 560$ s. (a): Inviscid slide. (b): Slide viscosity 2×10^7 Pa·s. (c): Free surface elevations along the cross section A-B of Frame (a).

(a)

(b)

(c)

(d)
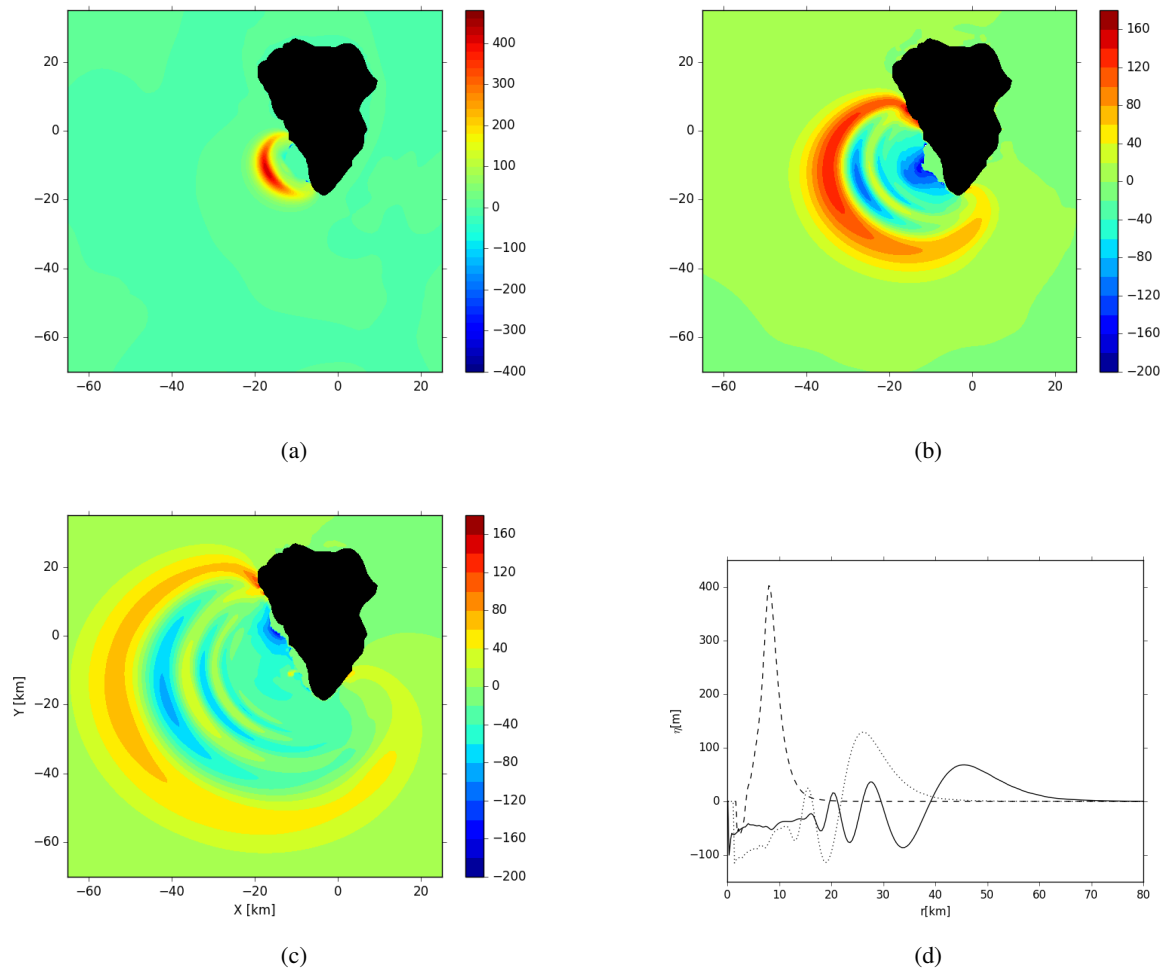
Figure 11. THETIS 3D computations for the 80 km^3 slide scenario. Contours of wave field at (a): t=102 s, (b): t=230 s, (c): t=342 s. (d): Free surface elevations along section A-B of Frame (a) of Figure 10. Slide viscosity 2×10^7 Pa·s.
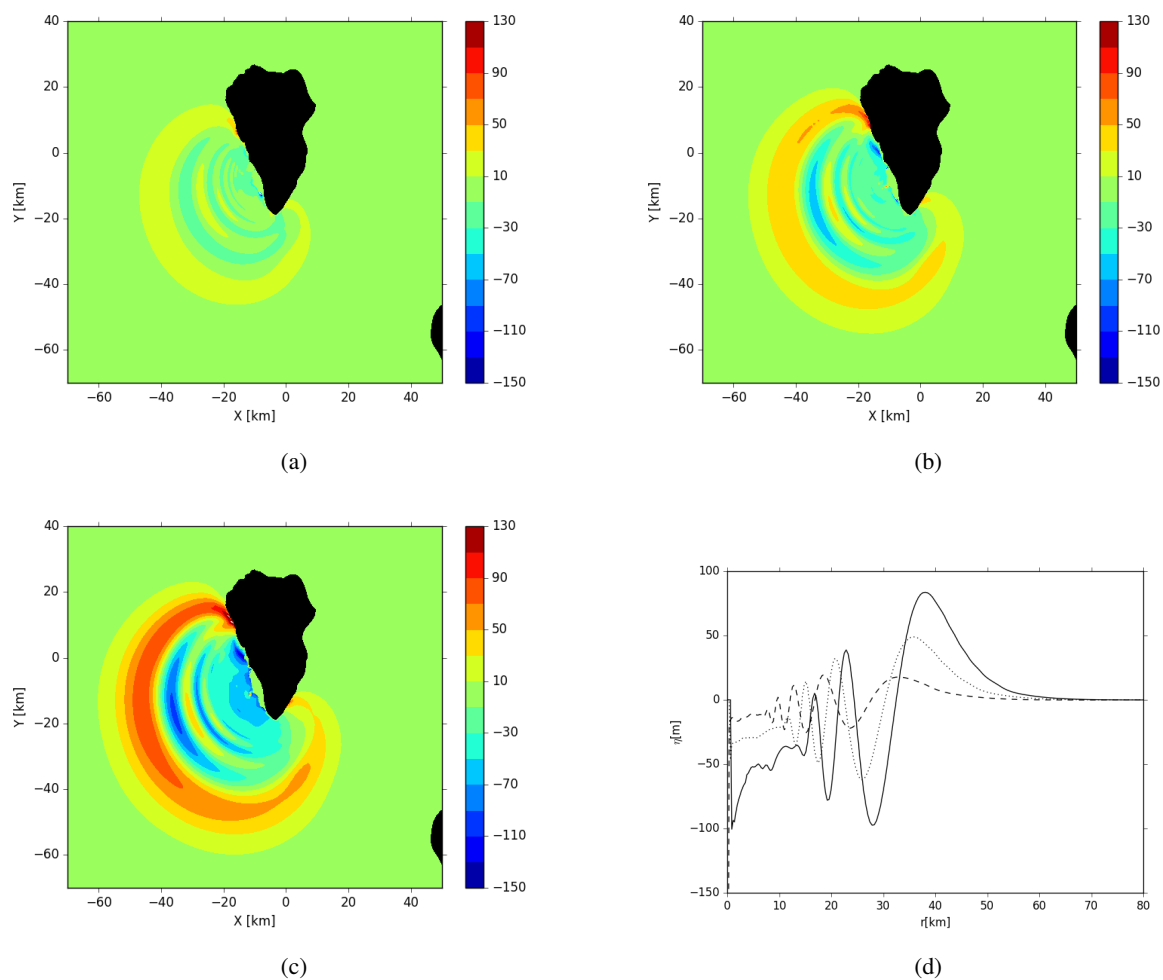
Figure 12. THETIS 3D computations for (a): 20 km^3, (b): 40 km^3 and (c): 80 km^3 slide scenarios at t=5 min. (d): Free surface elevations along section A-B of Frame (a) of Figure 10. Slide viscosity $2{\times}10^7$ Pa·s.

(a)   (b)
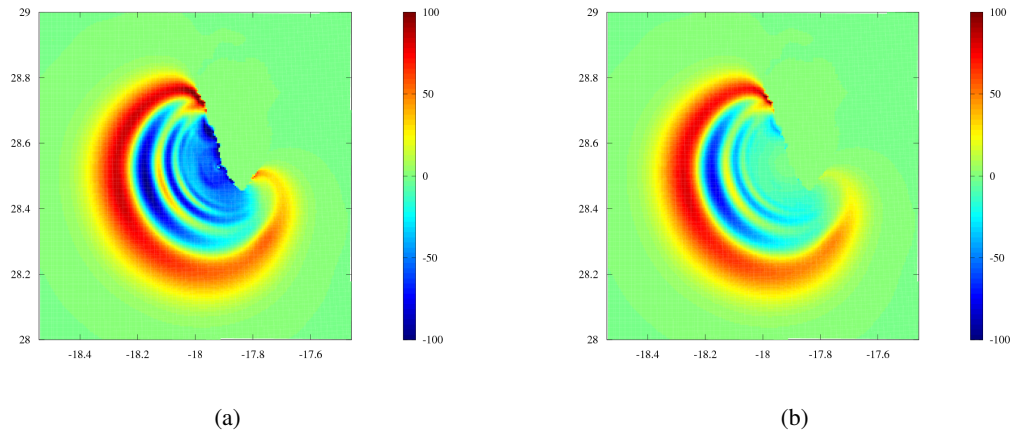
Figure 13. Region around Cumbre Vieja Volcano after 5 minutes of simulated time with THETIS for the 80 km^3 slide scenario. (a): Wave elevation for the initial solution from THETIS. (b): Filtered state which is used to initialize FUNWAVE-TVD.

(a)   (b)
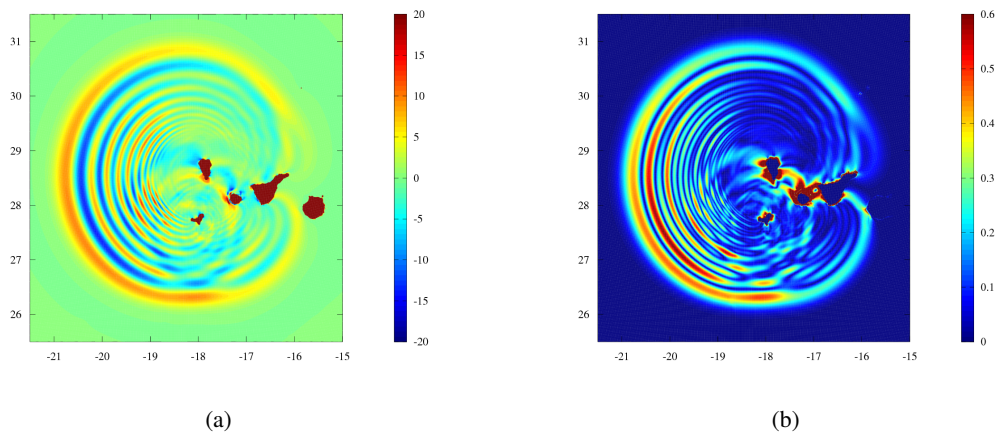
Figure 14. Region around the Canary Islands, 20 minutes after the beginning of the event (after 5 minutes of simulated time with THETIS, and 15 minutes of simulated time with FUNWAVE-TVD) during the 80 km^3 slide volume scenario. (a): Wave elevation. (b): Horizontal water velocity magnitude.
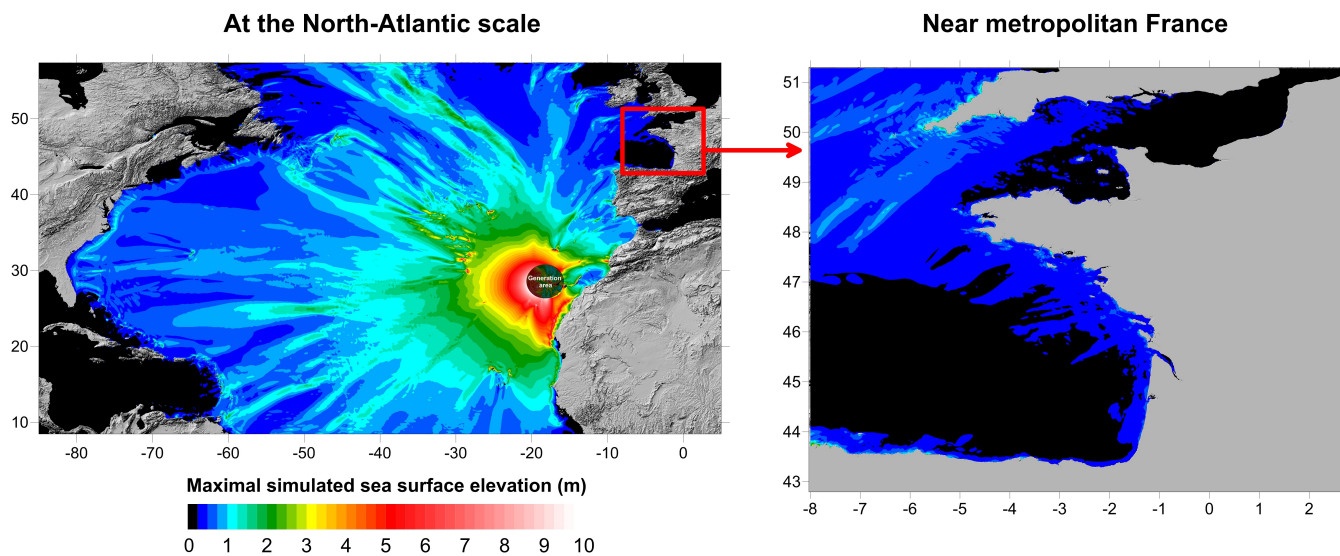
Figure 15. Maximum surface elevations (m) computed by FUNWAVE-TVD for the 80 km^3 scenario, from the generation area to the French coasts and other remote territories, with a 2.7-km resolution. The right picture represents a daughter grid covering the west French coasts, with a 450-m resolution.
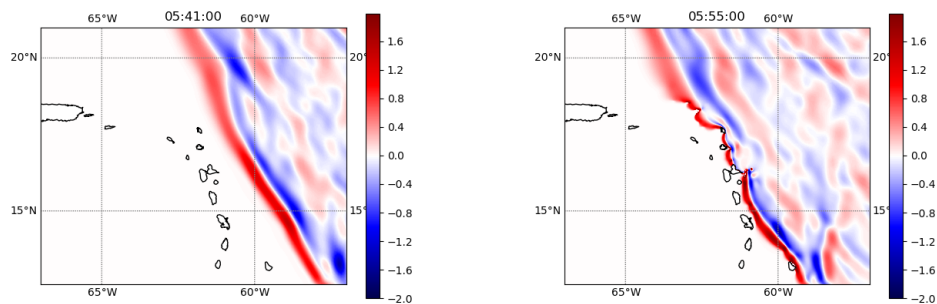
Figure 16. Surface elevations (m) computed by SCHISM around Guadeloupe and Martinique Islands for the 80 km^3 flank collapse scenario.
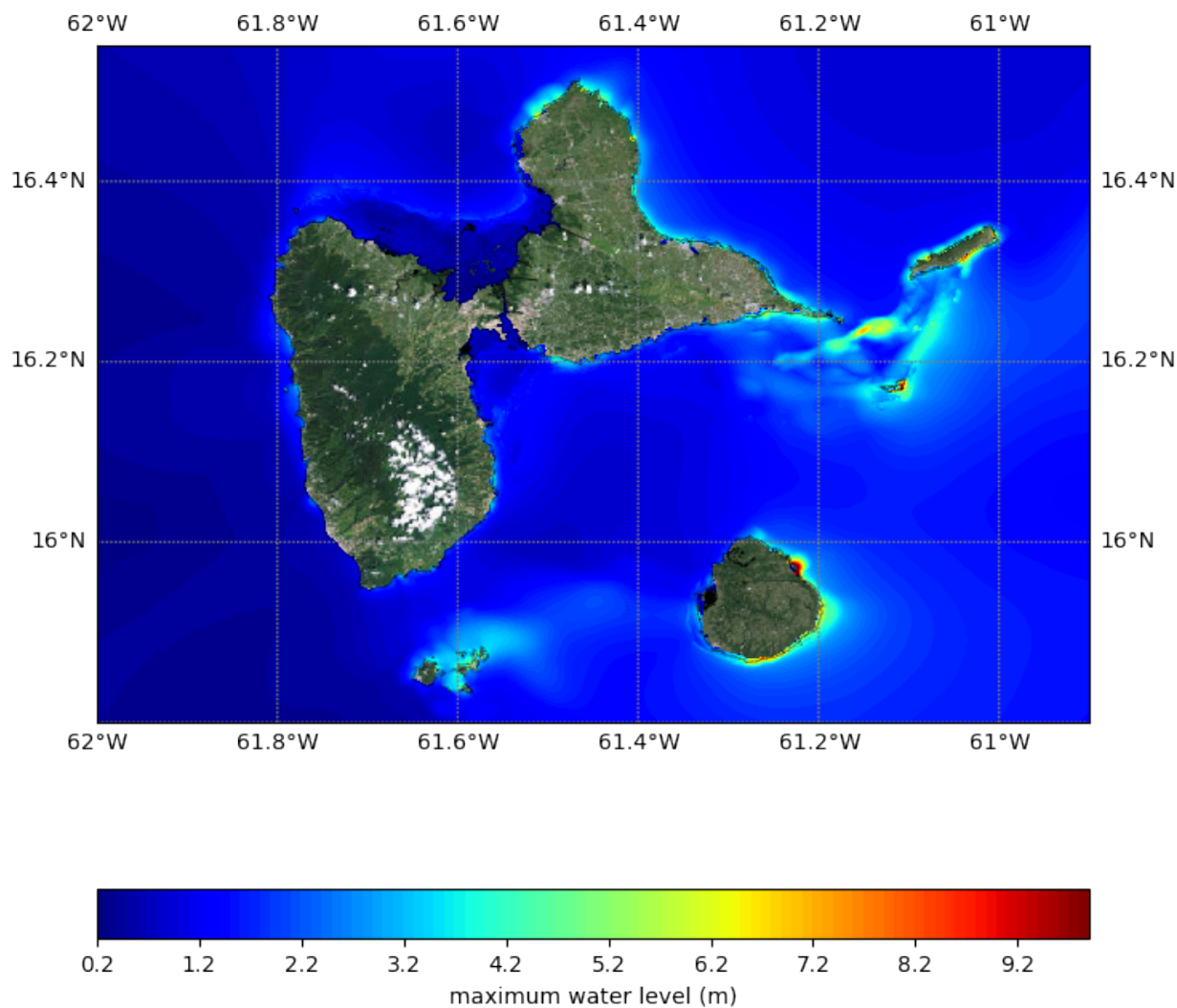
Figure 17. Maximum surface elevations (m) computed by SCHISM for the 80 km^3 scenario for the Guadeloupe Archipelago. Map created using ArcGIS® software by Esri. ArcGIS® and ArcMap™ are the intellectual property of Esri and are used herein under license. Copyright © Esri. All rights reserved
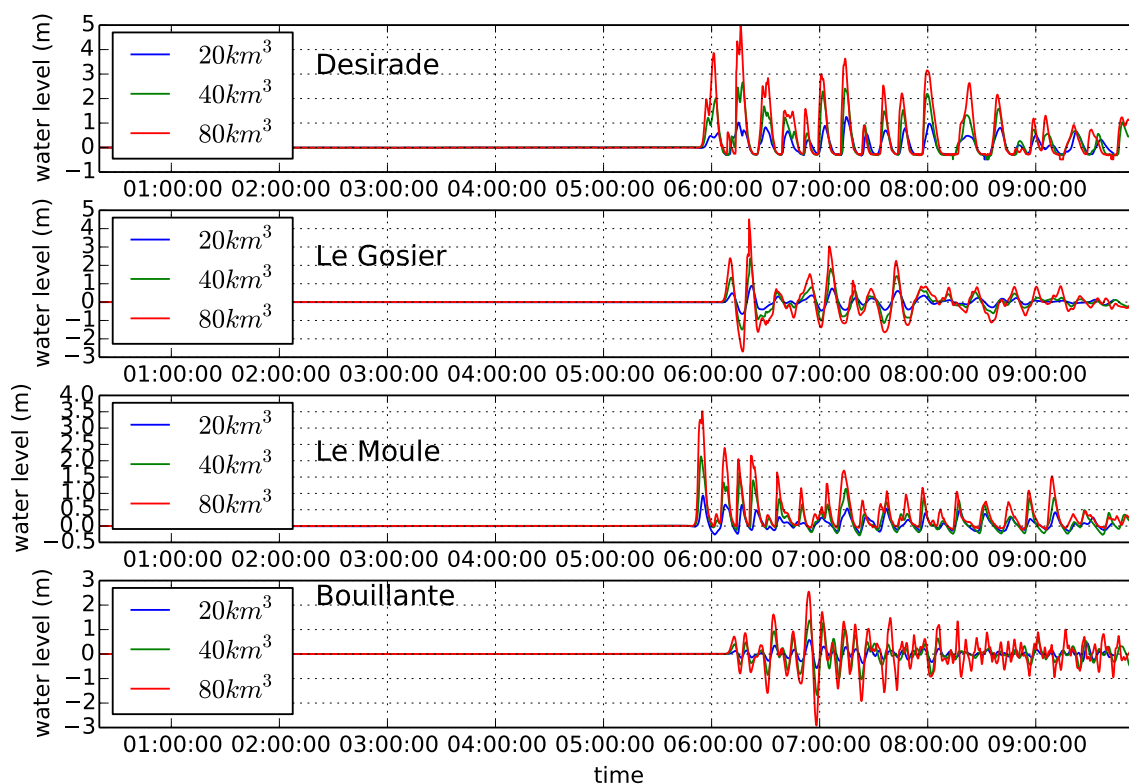
Figure 18. Surface elevations (m) for the 20, 40 and 80 km³ scenarios at the stations located on Figure 6 computed with SCHISM. The time takes into account the 20 first minutes of the slide and tsunami generation.
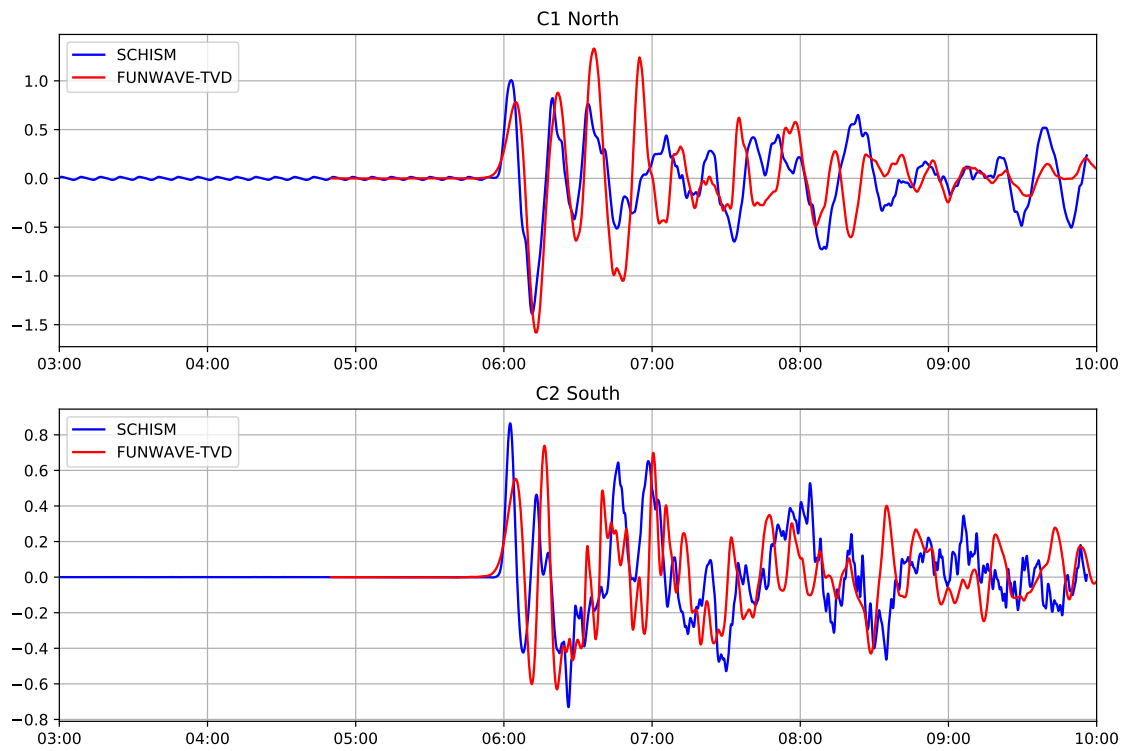
Figure 19. Comparison of the surface elevation (m) between SCHISM (blue) and FUNWAVE-TVD (red) in the vicinity of the Guadeloupe area, at the stations C1 and C2 mentioned on Figure 6 for the 80 km^3 scenario.
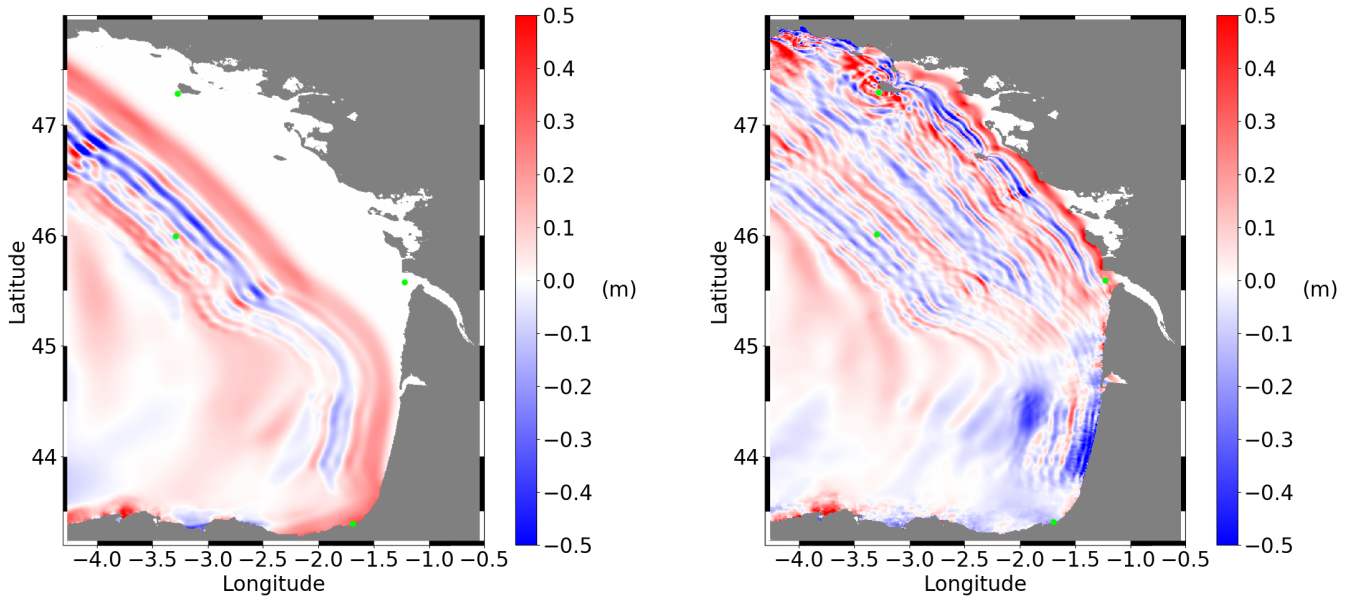
Figure 20. Wave train in the Bay of Biscay area for the 80 km^3 scenario, computed by Calypso. Left panel: 4 h after collapse, right panel: 5 h after collapse.
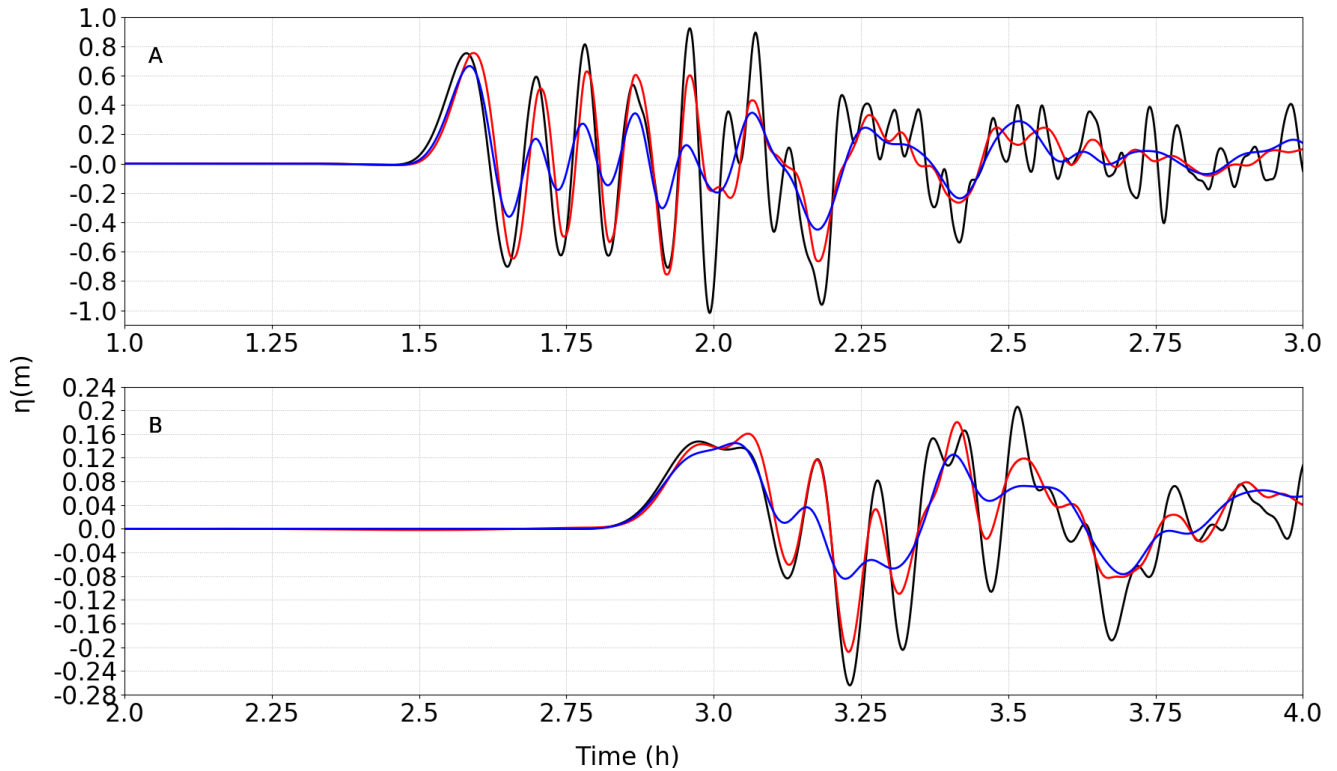
Figure 21. Surface elevations (m) for the 80 km^3 scenario at Gauge 1 in south Portugal (A) and Gauge 2 in the abyssal plain of the Bay of Biscay (B), computed by Calypso (black), FUNWAVE-TVD (red) and Telemac-2D (blue). The time takes into account the 20 first minutes of the slide and tsunami generation.
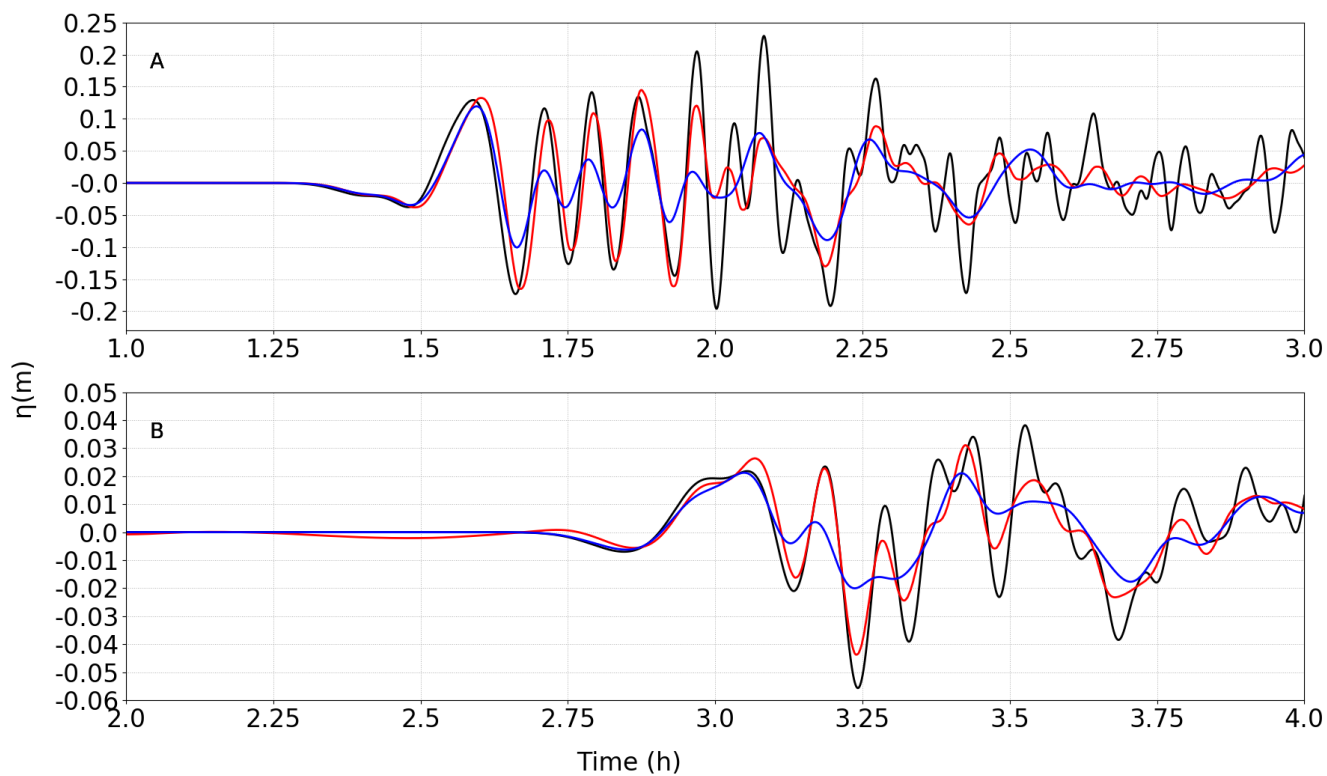
Figure 22. Same as in Figure 21 for the 20 km^3 scenario.
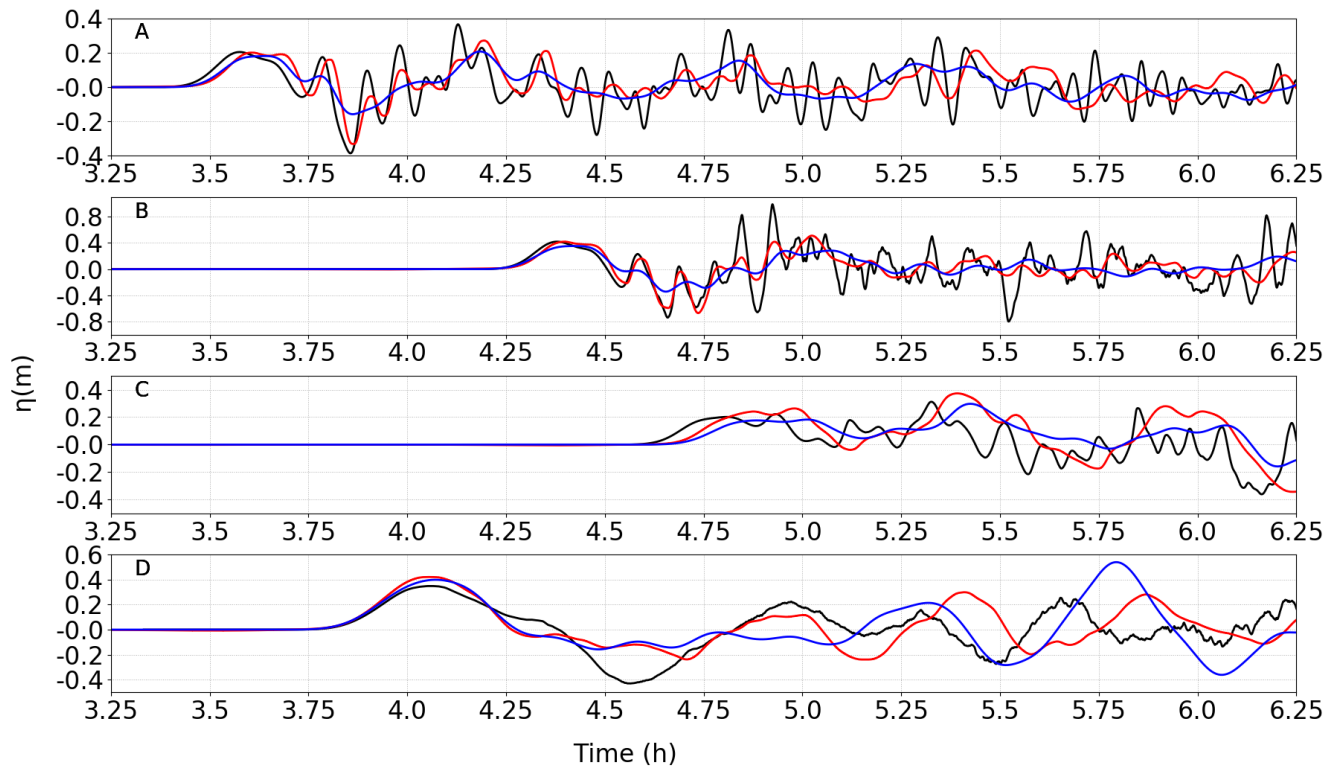
Figure 23. Surface elevations (m) for the 80 km³ scenario at Gauge 3 in the continental shelf of the Bay of Biscay (A), Gauge 4 in south Brittany (B), Gauge 5 in the Gironde estuary (C) and Gauge 6 in Saint-Jean-de-Luz (D), computed by Calypso (black), FUNWAVE-TVD (red) and Telemac-2D (blue). The time takes into account the 20 first minutes of the slide and tsunami generation.
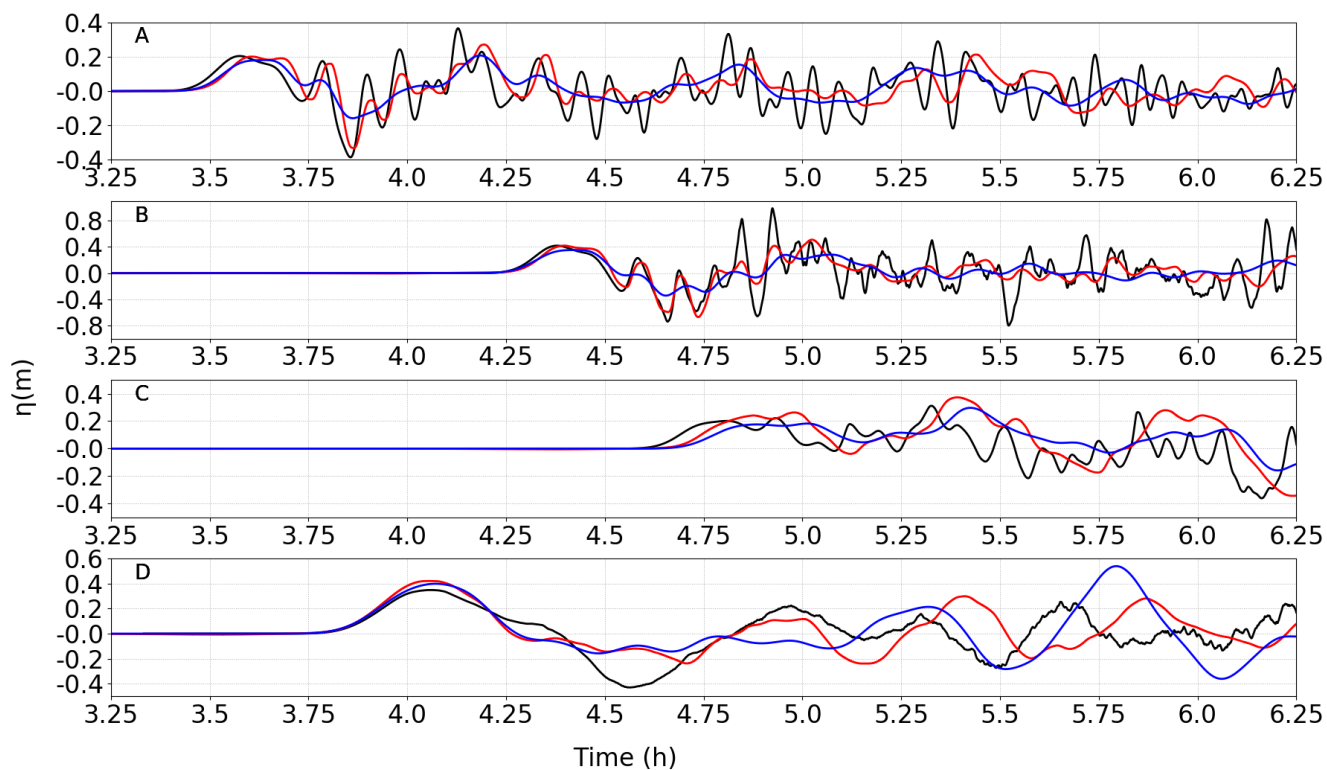
Figure 24. Same as in Figure 23 for the 20 km^3 scenario.
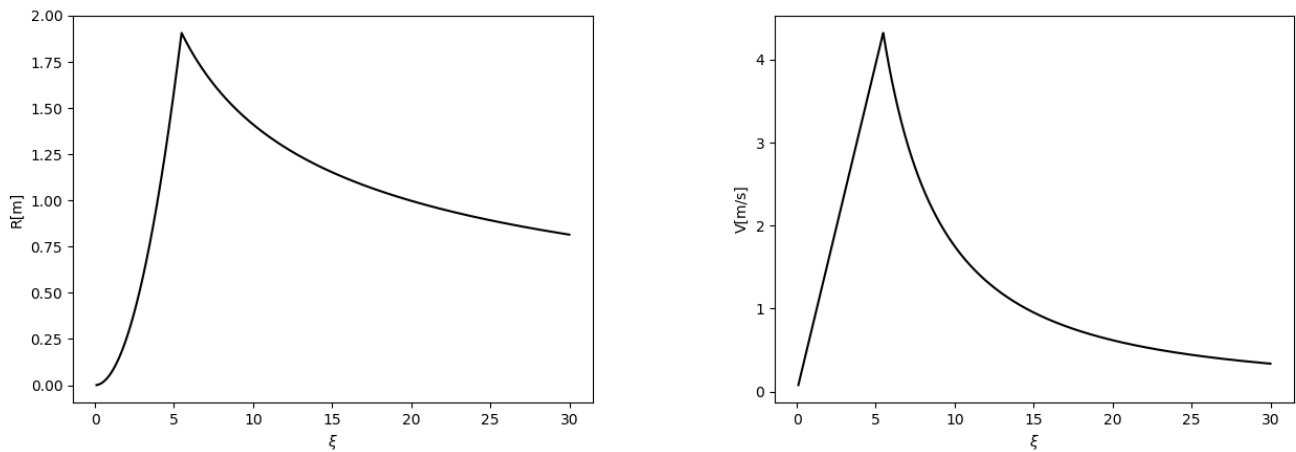
Figure 25. Run-up (left) and maximum flow velocity (right) estimated from Madsen and Fuhrman (2008) versus non-dimensional surf similarity parameter for the Atlantic coast of France considering the 80 km^3 scenario.
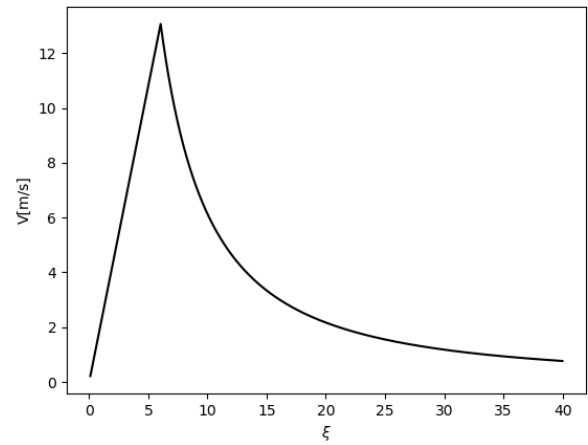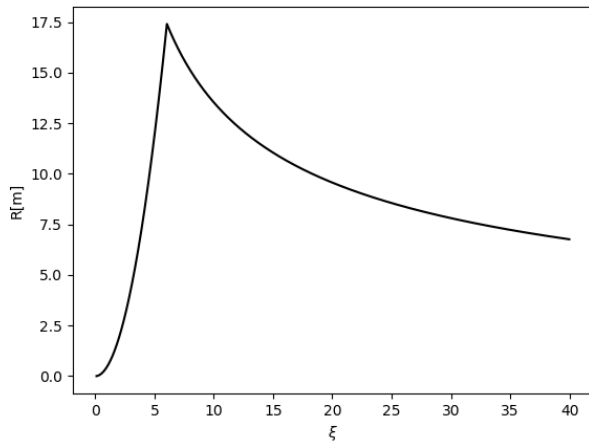
Figure 26. Same legend as Figure 25 for the Guadeloupe area.
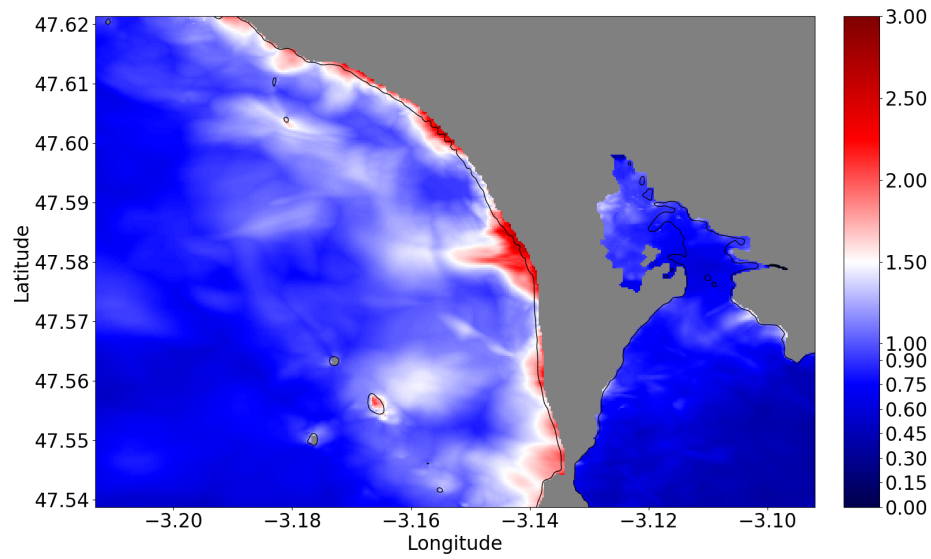
Figure 27. Maximal surface elevations and heights (m) in the flooded area (i.e., value behind the coastline represented by the black solid line) computed by Calypso in the Quiberon area, Brittany, French Atlantic coast.
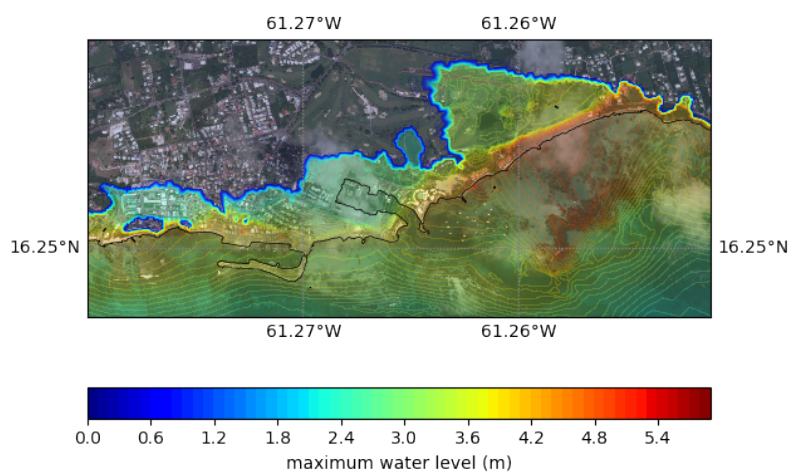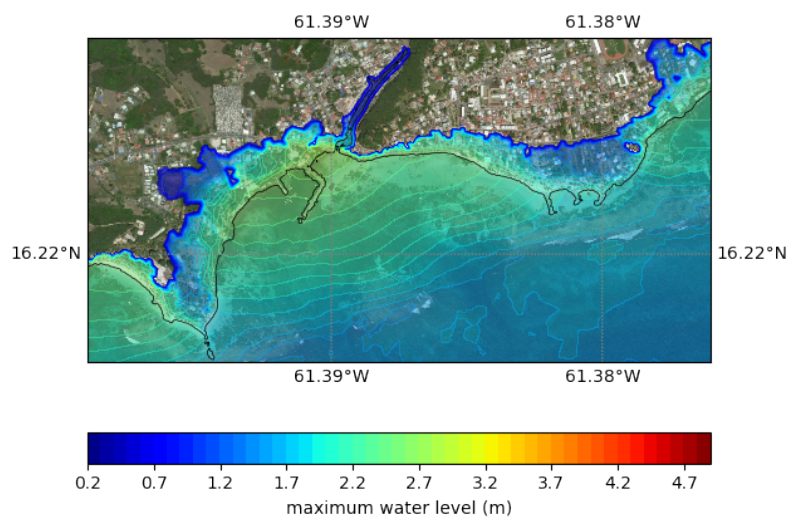
(a) (b)

Figure 28. Flood map showing the maximum water level reached during the 80 km³ scenario for the region of Sainte-Anne (a) and Saint-François (b) (see locations in Figure 6), computed by SCHISM. Map created using ArcGIS® software by Esri. ArcGIS® and ArcMap™ are the intellectual property of Esri and are used herein under license. Copyright © Esri. All rights reserved.
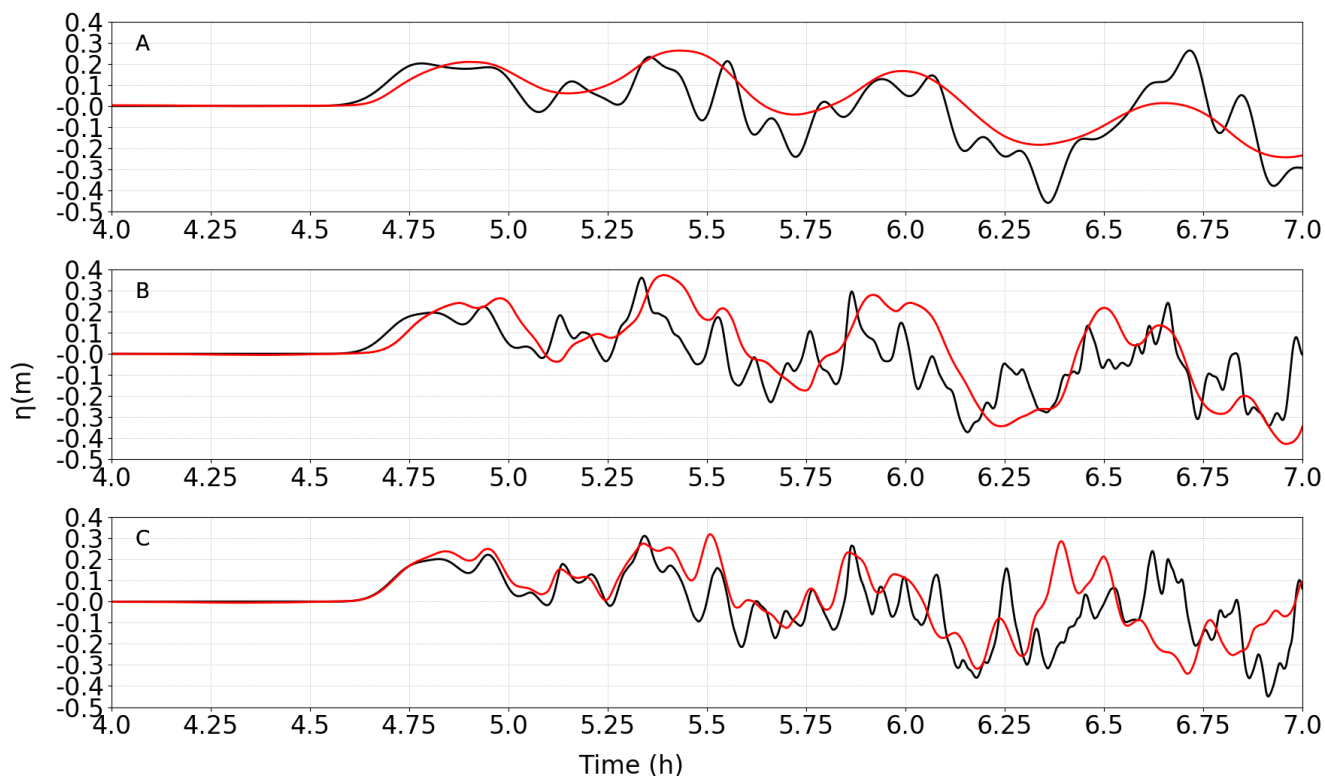
Figure 29. Comparison of the surface elevation (m) at Gauge 5 between Calypso (in black) and FUNWAVE-TVD (in red) for the 80 km^3 scenario at the Gironde estuary, for three resolutions: 2.7 km (A), 450 m (B) and 110 m (C) for FUNWAVE-TVD and 2 km (A), 500 m (B) and 125 m (C) for Calypso.
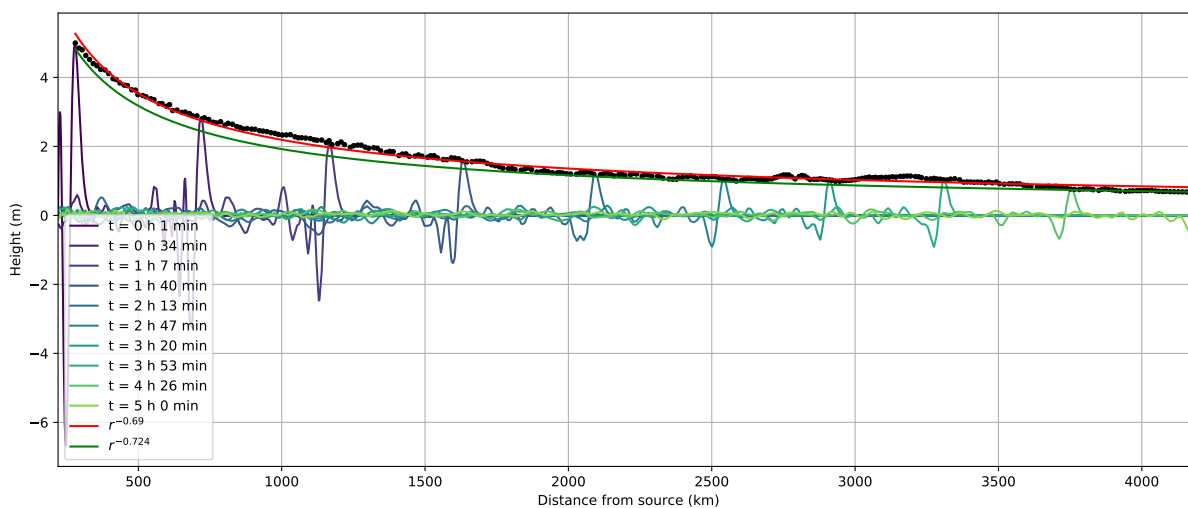
Figure 30. Surface elevation (m) at different times along the transatlantic transect of Figure 4 for the 40 km^3 scenario computed by the SCHISM model. Wave amplitude decay is shown at different rate for comparison.

Table 1. Summary of locations of numerical output

Gauge	Latitude	Longitude	Depth (m)
1	35.2247	-8.85923	3260
2	45.8663	-6.85191	4810
3	46.0016	-3.27661	130
4	47.2934	-3.26421	50
5	45.5854	-1.21069	10
6	43.3979	-1.67607	20